



Karolinska
Institutet

Karolinska Institutet

<http://openarchive.ki.se>

This is a Peer Reviewed Accepted version of the following article, accepted for publication in Cell Death & Differentiation.

2021-09-16

MTH1 as a target to alleviate T cell driven diseases by selective suppression of activated T cells

Karsten, Stella; Fiskesund, Roland; Zhang, Xing-Mei; Marttila, Petra; Sanjiv, Kumar; Pham, Therese; Rasti, Azita; Bräutigam, Lars; Almlöf, Ingrid; Marcusson-Ståhl, Maritha; Sandman, Carolina; Platzack, Björn; Harris, Robert A; Kalderén, Christina; Cederbrant, Karin; Helleday, Thomas; Warpman Berglund, Ulrika

Cell Death Differ. 2022 Jan;29(1):246-261.

Springer Nature

<http://doi.org/10.1038/s41418-021-00854-4>

<http://hdl.handle.net/10616/47733>

If not otherwise stated by the Publisher's Terms and conditions, the manuscript is deposited under the terms of the Creative Commons Attribution-NonCommercial-NoDerivatives License (<http://creativecommons.org/licenses/by-nc-nd/4.0/>), which permits non-commercial re-use, distribution, and reproduction in any medium, provided the original work is properly cited, and is not altered, transformed, or built upon in any way.

TITLE PAGE

MTH1 as a target to alleviate T cell driven diseases by selective suppression of activated T cells

Stella Karsten^{1*}, Roland Fiskesund^{1,2}, Xing-Mei Zhang³, Petra Marttila¹, Kumar Sanjiv¹,
Therese Pham¹, Azita Rasti¹, Lars Bräutigam^{1,4}, Ingrid Almlöf¹, Maritha Marcusson-Ståhl⁵,
Carolina Sandman⁵, Björn Platzack⁵, Robert A. Harris³, Christina Kalderén¹, Karin
Cederbrant⁵, Thomas Helleday^{1,6}, Ulrika Warpman Berglund^{1,7*}

Affiliations:

¹ Science for Life Laboratory, Department of Oncology-Pathology, Karolinska Institutet, 171 76 Stockholm, Sweden.

² Department of Medicine Huddinge, Karolinska Institutet

³ Applied Immunology and Immunotherapy, Department of Clinical Neuroscience, Karolinska Institutet, Center for Molecular Medicine, Karolinska University Hospital, Stockholm, Sweden

⁴ Comparative Medicine, Karolinska Institutet, 171 76 Stockholm, Sweden

⁵ RISE Research Institutes of Sweden, unit for Chemical and Pharmaceutical safety, 151 36 Södertälje, Sweden

⁶ Weston Park Cancer Centre, Department of Oncology and Metabolism, University of Sheffield, Sheffield S10 2RX, United Kingdom

⁷ Oxcia AB, Stockholm, Sweden

* Corresponding authors

Ulrika Warpman Berglund
+46-70 4329123; ulrika.warpmanberglund@scilifelab.se
Stella Karsten
+4672 0238614; stella.karsten@scilifelab.se
Science for Life Laboratory
Box 1031
171 21 Stockholm, SWEDEN

ABSTRACT

T cell-driven diseases account for considerable morbidity and disability globally and there is an urgent need for new targeted therapies. Both cancer cells and activated T cells have an altered redox balance, and up-regulate the DNA repair protein MTH1 that sanitizes the oxidized nucleotide pool to avoid DNA damage and cell death. Herein we suggest that the up-regulation of MTH1 in activated T cells correlates with their redox status, but occurs before the ROS levels increase, challenging the established conception of MTH1 increasing as a direct response to an increased ROS status. We also propose a heterogeneity in MTH1 levels among activated T cells, where a smaller subset of activated T cells does not up-regulate MTH1 despite activation and proliferation. The study suggests that the vast majority of activated T cells have high MTH1 levels and are sensitive to the MTH1 inhibitor TH1579 (Karonudib) via induction of DNA damage and cell cycle arrest. TH1579 further drives the surviving cells to the MTH1^{low} phenotype with altered redox status. TH1579 does not affect resting T cells, as opposed to the established immunosuppressor Azathioprine, and no sensitivity among other major immune cell types regarding their function can be observed. Finally, we demonstrate a therapeutic effect in a murine model of experimental autoimmune encephalomyelitis. In conclusion, we show proof of concept of the existence of MTH1^{high} and MTH1^{low} activated T cells, and that MTH1 inhibition by TH1579 selectively suppresses pro-inflammatory activated T cells. Thus, MTH1 inhibition by TH1579 may serve as a novel treatment option against autoreactive T cells in autoimmune diseases, such as multiple sclerosis.

INTRODUCTION

Autoimmune diseases constitute a large and heterogeneous group of different immunological diseases. They are mainly chronic and account for an extensive part of morbidity and disability in the developed world, with a prevalence of about 3-5% (1-3). Many autoimmune diseases, including multiple sclerosis (MS), are to a large extent T cell-driven (3-6). Thus, many current first-line treatment options comprise agents that directly affect T cells, such as Methotrexate (MTX) and Azathioprine (AZA), which both kill or inhibit proliferating cells non-specifically. Other examples from the treatment arsenal are more targeted therapies, like inhibition of specific cytokines and receptors by antibodies (e.g. anti-TNF), or small-molecular inhibitors (e.g. JAK1 inhibitors). However, depending on the disease and on local guidelines, AZA and MTX are often used as first-line treatments together with traditional anti-inflammatory treatments (e.g. glucocorticoids and non-steroidal anti-inflammatory drugs) (7-9). Although being crucial for patients with autoimmune diseases, these broadly acting drugs come with major side-effects, ranging from fatigue and nausea to severe infections, myelosuppression, organ toxicity, autoimmunity and demyelinating disease (10-12).

Despite the current knowledge and technical revolution within the field of immunology, there is still an urgent need for improved, targeted therapeutic strategies. Since T cells are also important in the defense against microbes and cancer, a successful new T cell targeting treatment ought to be well-balanced and specific to avoid severe adverse effects. It is commonly known that extensive depletion of T cells by drugs or conditions such as HIV infections increases the risk of both cancer and infections (13).

Reactive oxygen species (ROS) play a central role in both pathology and physiology (14, 15) and T cell signaling is ROS dependent (14-21), just like cancer cells have altered ROS status (22-24). However, elevated ROS levels as a consequence of dysfunctional redox regulation can cause DNA damage by oxidizing DNA directly or via bases in the deoxynucleoside triphosphate (dNTP) pool (25), ultimately leading to mutations. The human MutT Homolog 1 (MTH1 or NUDT1) sanitizes the cellular dNTP pool by turning oxidized dNTPs into dNMPs, therefore preventing oxidized nucleotides from being incorporated into DNA (26-29). However, MTH1 is not essential for cells, as MTH1 gene-depleted mice live to old age, despite a slightly increased mutational burden (30).

Already in 1997 it was reported (31) that the expression of MTH1 is up-regulated in T cells activated with phytohemagglutinin as compared to non-activated T cells, although the level is somewhat lower than in Jurkat cells (immortalized acute leukemia cells). Within the field of cancer research, a novel small-molecular inhibitor of MTH1 – TH1579 (Karonudib) – was recently introduced as a new promising treatment for cancer (32-35). Similar to activated T cells, MTH1 is up-regulated in many cancer cells, and oxidative stress sensitizes them to MTH1 inhibition (36). Targeting MTH1 in the context of cancer showed encouraging results and TH1579 was selected (33) for clinical trials for both solid tumors and leukemias (NCT03036228 and NCT04077307).

In this study we wanted to confirm the correlation between oxidative stress and MTH1 up-regulation in activated T cells. We hypothesized that like cancer cells, activated T cells would be sensitive to MTH1 inhibition by TH1579, and thus targeting MTH1 could be a new

treatment strategy against autoimmune diseases. We also speculated that, considering the heterogeneity among T cells (37, 38), possibly not all T cells are equally sensitive to MTH1 inhibition, and wanted to investigate the MTH1 level and ROS status in any surviving T cells. To further investigate the significance of TH1579 in autoimmunity, we tested TH1579 treatment in a murine model of MS, experimental autoimmune encephalomyelitis (EAE), and investigated drug toxicity in other immune cells.

Herein we demonstrate a selective T cell suppressive role of TH1579, with dose-dependent effects on the survival of pathologic T cells comparable to the established drug MTX, and more potent and specific than AZA. The doses needed for a therapeutic effect are in general non-toxic and well tolerated, with advantageous pharmacokinetic properties (33). We suggest that TH1579 could be used for treatment of T cell-driven diseases, and demonstrate the existence of MTH1^{high} and MTH1^{low} proliferating T cells.

RESULTS

MTH1 correlates with ROS status but is up-regulated before the redox status is altered

We first investigated MTH1 levels in activated *versus* resting T cells, and how they correlated with redox status. T cells from buffy coats of healthy donors were enriched and activated with CD3/CD28 beads and IL-2. In concordance with previous work (31), MTH1 was specifically up-regulated in activated T cells, whereas resting cells expressed a significantly lower level of MTH1 (Fig. 1A-C). As activated T cells have elevated ROS as a physiological feature (14-17), we investigated the ROS status and MTH1 levels with flow cytometry. The level of oxidative stress was as expected significantly increased upon activation in a time-dependent manner and correlated with MTH1 expression levels (Fig. 1A, D-G). However, MTH1 increased already within 24h upon stimulation (Fig. 1B-G, S1), whereas the major increase in ROS status was observed after 48-72h. This could indicate that either MTH1 is up-regulated as a direct response to T cell receptor (TCR) activation and downstream pathway signaling, before a persistent change in ROS status occurs, or that the elevated ROS pressure is compensated for during the first days, resulting in lower general redox status and thus reduced oxidation of the redox dye. MTH1 expression was consistent in all new generations of cells after 96h (Fig. 1H-I) and did not differ between CD4 and CD8 T cells (Fig. S2A-B).

Activated T cells are sensitive to TH1579

Following observation of elevated MTH1 levels in activated T cells, their sensitivity to MTH1 inhibition by TH1579 was investigated. We started by confirming target engagement of TH1579 to MTH1 using a temperature-dependent Cellular Thermal Shift Assay (CETSA), (Fig. 2A). Next, activated CD3+ cells were treated with TH1579 for 96h (Fig. 2B). We observed that

TH1579 suppressed the viability of activated T cells at nanomolar ranges (IC₅₀ 0.6 μ M) and that this effect was comparable to that of MTX in potency and selectivity, while being more selective and potent than AZA (Fig. 2C). Resting cells were unaffected by exposure to TH1579. CD4⁺ and CD8⁺ T cells were equally sensitive (Fig. 2D), with an increased proportion of apoptotic cells (Fig. 2E-F). Staining for the CD71 activation marker revealed significant elimination by TH1579 (Fig. 2G-H), indicating a reduced amount of live CD71⁺ cells, possibly due to selection. There was no difference in apoptosis or CD71 expression between CD4⁺ and CD8⁺ cells (Fig S2C-E) and we saw a similar trend with other activation markers like CD69 and CD25 (Fig. S3). When resting cells were stained with Carboxyfluorescein (CFSE) and then treated and stimulated simultaneously for 96h, we observed a dose-dependent correlation with the fraction of living cells not proliferating (Fig. 2I-K, S2F-G).

Taken together, these results suggest that MTH1 inhibition with TH1579 not only kills activated T cells, but also limits the number of proliferating cells in a dose-dependent manner.

TH1579 induces DNA damage and cell cycle arrest in replicating cells

To elucidate the mechanism through which the T cells die and undergo apoptosis, we investigated cell cycle and DNA damage. To follow the cells in S-phase during the initiation of the treatment, T cells were pulse-labelled with 5-Ethynyl-2'-deoxyuridine (EdU) prior to 4h (Fig. S4) or 24h (Fig. 3 and S4) of TH1579 treatment (Fig. 3A). As illustrated in Figure S5, the EdU positive cells made up less than 15 % of all cells after 24h, and thus the effect could be highlighted by gating for the EdU positive cells. We observed that after 24h, proliferating T cells were arrested in the G2/M phase and died (Fig. 3B-D, S4K-L). The population of SubG1

cells matched the experiments with Annexin and Sytox (Fig. 2E-F vs. Fig. 3C), where the fragmented cells in SubG1 corresponds to the late apoptotic and necrotic cells at 24h in Fig. 2E-F.

γ -H2AX was increased in activated T cells treated with TH1579 (Fig. 3E-G, S4M-P), and the majority of the γ -H2AX positive cells were in G2/M phase (Fig. 3E, G). The control Etoposide showed a strong but more even distribution of DNA damage in the different cell cycle phases, despite its known G2/M driving effects (Fig. 3E-G). The effect of TH1579 was altogether most prominent in EdU positive cells, indicating a strong sensitivity in the cells that were in S-phase during the initiation of the treatment (Fig. 3E-G, S4A, S4E-J, S4K, S4M-P). The accumulation of cells in the SubG1 pool was mainly caused by transfer from the EdU positive population (Fig. S5).

To investigate whether the cells reached mitosis or not, we stained the cells for Histone H3pS10 (Fig. 4A-D). In concordance with our previous data (39), we saw an increase of Histone H3pS10, in a similar manner to cells treated with the tubulin destabilizing agent Vincristine. Thus, we conclude that disruption of the mitotic spindle is contributing to the toxic effects of MTH1 inhibition. Similar effects have been seen in cancer cells, both by MTH1 inhibition and by MTH1 silencing (39, 40).

Using a modified COMET assay, we also verified that 8-oxo-guanine (8-oxoG) was significantly increased in activated T cells treated with TH1579 (Fig. 4E-G), potentially contributing to the toxicity of MTH1 inhibition.

MTH1^{high} T cells are sensitive to TH1579, whereas a subpopulation consisting of proliferating MTH1^{low} cells with lower ROS status show lower sensitivity

To demonstrate the correlation between MTH1 levels and sensitivity to MTH1 inhibition, we investigated the cell cycle and MTH1 levels in resting and activated cells. As previously known, resting cells do not proliferate and only express low levels of MTH1. Surprisingly, we found that a subset of MTH1^{low} cells proliferated and were less sensitive to TH1579 (Fig. 5A-B). The fraction of proliferating cells was lower in the MTH1^{low} population, and TH1579 appeared to have a slight effect on the cell cycle of also MTH1^{low} cells (Fig. 5C-G), but the sensitivity of MTH1^{high} cells was considerably higher. Furthermore, the distinction between resting cells and MTH1^{low} cells was evident when studying the cell cycle phases (Fig. 5F-G).

To investigate the effect on redox status and MTH1 expression, we measured MTH1 levels in T cells upon treatment with TH1579 (Fig. 6, S6). TH1579 drove the surviving T cell population towards the MTH1^{low} phenotype (Fig. 6A-D, S6A-B). Investigating the MTH1 levels of specific cell generations after 96h, we observed that the MTH1 levels were significantly decreased in later generations of living cells upon TH1579 treatment (Fig. 6E-F).

These findings cumulatively suggest that the inhibitor not only kills activated T cells, but also drives the remaining T cell population towards a phenotype with lower ROS and lower MTH1 levels, together with a decreased, but not abolished, propensity to proliferate.

TH1579 does not impair the function of human NK cells, monocytes or neutrophils, and has a transient effect on antibody production in rats at high doses

As many current immunosuppressive drugs impair the immune system broadly with possible life-threatening consequences (10-13), we wanted to investigate any potential suppressive effects on other immune cell types than T cells. According to our observations, TH1579 does not suppress phagocytosis by monocytes or neutrophils, nor does it suppress oxidative burst (Fig. 7A-D). NK cells maintained their capacity to kill their K562 target cells upon treatment with TH1579 up to 12 μ M (Fig. 7E-F). The concentrations used were well within the plasma exposure for efficacy in the EAE model described further below.

To investigate B cell function, we treated rats with TH1579 and measured their primary and secondary antibody responses (IgG and IgM) on immunization with keyhole limpet hemocyanin (KLH), both during treatment and a following recovery period (Fig. 7G). Antibody production was suppressed at the highest dose, whereas the animals that had recovered after the treatment period showed a fully functional antibody production capacity (Fig. 7G-K). Considering hematological aspects, animals treated with the highest dose presented with leucopenia during treatment, yet that effect was reversible (Tabl. S1A-B). These results indicate that high doses of TH1579 have a transient, reversible suppressive effect on the bone marrow.

TH1579 improves the clinical status of mice with EAE and suppresses MOG-specific effector memory T cells

To test the therapeutic effects of TH1579 in a T cell-driven disease model, we employed a murine MS model of EAE induced by myelin oligodendrocyte glycoprotein (MOG). In the model, mice are immunized with MOG, causing T cell driven inflammation in the central nervous system. Following immunization (day 0), the mice were treated with TH1579 from

either day 1 or when the onset of disease symptoms occurred on day 12. When treated from the onset of symptoms (day 12), TH1579 did not affect disease progression, but the recovery of TH1579 treated mice was significantly improved compared to that of the untreated group (Fig. 8A). When starting the treatment from day 1 post-immunization, TH1579 could either prevent the disease developing or significantly alleviate the disease symptoms (Fig. 8A). The therapeutic effects of TH1579 were also demonstrated by comparing cumulative scores between the treated and un-treated groups (Fig. 8B). This indicates that while the effect of the drug is strongest prophylactically, it also shortens the recovery period when given at the onset of symptoms.

Furthermore, CD4⁺ effector memory T cells were reduced in animals treated subcutaneously with TH1579 (Fig S7), supporting the hypothesis that TH1579 indeed operates on activated T cells induced through MOG immunization. To further investigate this, mice were immunized and treated from day 1 (Fig 8C). At day 23, the splenocytes of experimental mice were stimulated *ex vivo* with either vehicle, MOG or Concanavalin A (ConA). In concordance with the previous KLH immunization studies in rats, T cells were not impaired in their ability to proliferate on ConA (Fig 8D). However, there was a significant difference in the recall response to the specific antigen MOG (Fig. 8D), suggesting that TH1579 suppressed the effector memory T cells during the induction of the disease, which could well explain the better clinical outcome among the treated mice.

In summary, we provide proof of concept for MTH1 as a target and TH1579 as a novel treatment for T cell-driven diseases, by using *in vitro* and *in vivo* approaches. The EAE data

suggest that the effect of the inhibitor is strongest if given prophylactically, but it also has an effect if given after onset of symptoms.

DISCUSSION

Herein we demonstrate TH1579 as a new approach to selectively suppress T cells in T cell-driven diseases and compare it with the established drugs MTX and AZA. This is the first time the anti-inflammatory properties of TH1579 with inhibition of MTH1 are demonstrated in human T cells and an animal model of EAE, complementing recent findings in a psoriasis setting (41) and acute autoimmune hepatitis (Chen *et al.*, submitted). While the up-regulation of MTH1 in activated leukocytes has been previously described (31), the demonstration of heterogeneity of MTH1 levels and sensitivity to MTH1 inhibition among activated T cells are novel findings.

It is still not proven if the rise in number of MTH1^{low} T cells is caused by differentiation driven by TH1579, or if they are selected from a smaller, already existing population less sensitive to TH1579, but the data in Fig. 5 suggest the latter. The MTH1^{low} cells are also confirmed to be distinguished from resting cells, but their functions and traits are yet to be explored. Considering the good clinical outcome in the *in vivo* data despite the lower sensitivity of MTH1^{low} cells among proliferating T cells, MTH1^{low} cells could be less pro-inflammatory. Thus, the resistant cells might not cause clinical issues such as in a cancer setting (42), possibly even the opposite with some preserved immunity instead.

The differentiation of T cells into separate subsets is to a large part controlled by ROS signaling and metabolic programming (5, 43-48). It is thus plausible that MTH1 inhibition could have an immunomodulating role via ROS-dependent and related metabolic effects (36) and subset polarization not investigated herein. Although ROS is classically associated with inflammatory processes, the complexity of the subject has been illustrated by several studies

(49, 50). Elucidating the potential difference in sensitivity among T cell subsets and the correlation to MTH1 levels is thus important to predict any yet unseen downsides and advantages of MTH1 inhibition. It would be of great interest to investigate an MTH1^{-/-} immune system as well as the MTH1^{low} cells regarding cell subsets, cytokine profile, functional assays and metabolic profiling. A skew towards suppressing mainly T regulatory cells could cause even more inflammation, although the role of T regulatory cells is diverse and controversial (51, 52). Our *in vivo* experiments do not suggest such a pro-inflammatory secondary consequence (Figure 8), although the effect could be more subtle with associated cancer, or tissue/disease specific adverse effects.

Oxidation of DNA and its building blocks could be regarded as a quick but rough evolutionarily well-preserved signaling mechanism. Guanine has the lowest redox potential of the DNA bases, making it vulnerable to oxidation (53), and as shown in the COMET assay, MTH1 inhibition increases 8-oxoG levels in ROS-rich T cells. The DNA glycosylase 8-Oxoguanine DNA Glycosylase (OGG1) excises 8-oxoG from the DNA (54-56) and has been described to be strongly associated with immune responses (57-63), serving as an example of another DNA repair enzyme intrinsically involved in inflammation. Hypothetically, MTH1 could itself serve as an important inflammatory messenger either directly or indirectly. It could be up-regulated as a direct response to the highly ROS-dependent TCR stimulation, rather than MTH1 only responding to the generally increased ROS as suggested in earlier studies (32). The fact that the MTH1 levels were already elevated after 24h, whereas the major change in ROS status followed later, could support this theory. Some data even suggest a direct effect on microtubule polymerization (39), which would raise the question what immunomodulatory effects other established tubulin-affecting agents have.

Increased DNA damage and oxidative stress is described to be immunogenic and promote inflammatory signaling (64-69), but the correlation is complex. Elevated 8-oxoG due to MTH1 inhibition would expectedly cause more inflammation via OGG1 and other DNA repair pathways. OGG1 levels are indeed elevated in many inflammatory diseases, whereas MTH1 expression remains somewhat unclear (70, 71). Conversely, 8-oxoG is also considered to drive carcinogenesis via mutagenesis, but nevertheless the opposite was observed in mice in which both OGG1 and MTH1 were gene-deleted, despite higher 8-oxoG (72). The findings in the double MTH1-OGG1 KO mice illustrate the controversial role of these DNA repair enzymes for mutations and cancer. Nevertheless, the potential cancer risk due to increased mutations is a disturbing aspect of inhibiting a DNA repair enzyme. Even though MTH1 KO mice only have a slightly increased tumor rate, the situation might be different for humans who live much longer. However, also MTX (10) and AZA (73) increase the cancer risk over time, both by inducing mutations and by their broad immunosuppressive effects. Equally the beneficial effects of MTH1 inhibition might still overcome the adverse effects. As activated T cells are short lived as compared to most other cells of the body, the window for potential mutations to originate is expected to be much smaller than for established drugs that affect all dividing cells non-specifically, and still are suitable for chronic treatment.

Altogether, our *in vitro* results indicate that many pro-inflammatory T cells are depleted upon treatment with TH1579, but the relationship between ROS, MTH1, the DNA damage response and inflammation remain controversial. More studies on the direct effects of altered ratios in the dNTP pool, oxidized nucleotides, excised free oxidized bases, and ATP- and GTPases are needed, especially in non-cancerous cells. Several established drugs, like

antifolates and nucleotide analogs, already affect nucleoside and nucleotide metabolism with anti-inflammatory, anti-cancerous and anti-viral effects (74-76).

Regarding the risk of excessive immunosuppression, we show that TH1579 is selective for activated T cells, the effect is reversible after ending the treatment, and that other cells of the immune system seem unaffected. Furthermore, it has previously been demonstrated that TH1579 does not suppress the cytotoxic activity of tumor-infiltrating lymphocytes at doses efficient against cancer and tumors (77). It is thus plausible that TH1579 is not inferior to other established drugs regarding side-effects on the bone marrow.

Our study shows proof of the therapeutic concept in the well-established EAE animal model. The risk of becoming dependent on a wheelchair within 25 years of disease onset in MS is still 50%, and the typical age for disease onset of the T cell-driven disease is 30 years of age (78, 79). We show that the effect of the MTH1 inhibitor is most prominent prophylactically, which could favor maintenance treatment, but in addition the improvement when administered after obvious symptoms indicates potential for shortening relapse episodes and improving recovery. Many patients present their symptoms in the form of relapses, rather than continuous manifestations (78), which is not unique for MS among autoimmune diseases. In addition to MS, there are many other T cell-driven diseases, not least those in which MTX and AZA are first-line treatment options, where MTH1 inhibition could be a promising new addition to the therapeutic strategies.

MATERIALS AND METHODS

All *in vitro* experiments with human samples were made on material from at least 3 different individuals and with a minimum of technical duplicates for each experiment. This was to ensure statistical quality. For animal studies the animal groups were bigger (minimum $n=7$), as stated in the figure legends and description of Materials and Methods for each experiment further below. This was to maintain statistical quality despite the higher natural variation between animals as compared to replications of *in vitro* experiments. The variation is illustrated with error bars, showing the standard deviation, illustrating that the variance was typically within the same order of magnitude between comparable groups, except for in cases where the control group was normalized to 1.0 for each replicate. No statistical estimation of sample size was performed. Pre-established criteria for exclusion were stated in the ethical permit, on ethical grounds, but no animal was excluded from the study. None of the experiments in this work involved moments where the investigator was blinded.

The stock solution of TH1579 was 10 mM in DMSO. 0.05% DMSO was used as control, corresponding to the highest concentration of 5 μ M in the compound formulation.

Flow cytometry was performed using either a Novocyte 3000 (Agilent, Santa Clara, CA, United States), Novocyte Quanteon 4025 (Agilent, Santa Clara, CA, United States), Navios (Beckman Coulter, Brea, CA, United States), Gallios (Beckman Coulter, Brea, CA, United States) or FACSCantoII (Becton Dickinson, Franklin Lakes, NJ, United States) and analyzed with FlowJo™ (Becton Dickinson, Franklin Lakes, NJ, United States), FACSDiva™ (Becton Dickinson) or Kaluza (Beckman Coulter, Brea, CA, United States) software. Single stain controls for compensation using compensational beads (552843, Becton Dickinson) were

used for antibodies. Fluorescent minus 1 (FMO) controls were used to ensure positive gating although the final gate was set individually for each experiment according to the experiment setup and biological control in addition to the FMO control.

Cell preparation, activation and culture

T cells from healthy donors were obtained fresh from the buffy coats of healthy donors, via the Karolinska Hospital in Stockholm, Sweden. T cells were enriched using RosetteSep™ Human T Cell Enrichment Cocktail (15028, StemCell technologies), SepMate™-50 separation tubes (85458, StemCell technologies) and density media Ficoll Paque Plus (17-1440-03, Ge Healthcare) according to the manufacturer's instructions. The cells were cultured in RPMI 1640 + Glutamax medium (61870-044, Thermo Fisher Scientific) supplemented with 10 % FBS (10500064, Thermo Fisher Scientific) and 50 U/mL penicillin/streptomycin (15070063, Thermo Fisher Scientific) at 37°C and 5% CO₂. Cells were typically activated within 24h of separation, with Dynabeads™ Human T-Activator CD3/CD28 (11131D, StemCell technologies) using 0.75 beads per cell, and 25 ng/μL IL-2 (PHC0027, Thermo Fisher Scientific). Activated T cells were seeded at a concentration of 0.8 million/mL and resting were kept in culture at 1-2 million/mL. When seeded for expansion 96h prior to drug treatment, cells were seeded into T25 or T75 flasks with ventilated caps (83.3911.502, Sarstedt) and X1 fresh medium with new IL-2 was added after 48h. For treatment with compound, T cells were seeded into round-bottomed 96 well plates (83.3925.500, Sarstedt). Cells were counted using a TC20™ Automated Cell Counter (Bio-Rad) and 0.4 % Trypan blue (1450021, Bio-Rad).

CETSA

2 million pooled activated T cells were treated with either 10 μ M TH1579 or 0.1% Dimethyl sulfoxide (DMSO) for 1h at 37°C. Cells were then distributed into 12 different tubes and incubated at 12 different temperatures from 37°C to 60°C for 3 min, and immediately cooled thereafter. The samples were then used for Western blot analyses as described below. The band intensity was normalized to the DMSO control at 37°C for each sample.

Western Blot MTH1 levels

Any dynabeads were magnetically removed and cells were diluted in RIPA buffer (150 mM sodium chloride, 1 % NP-40, 0.5 % sodium deoxycholate, 0.1 % sodium dodecyl sulfate, 50 mM Tris pH 8.0) with 1X cOmplete™ Protease Inhibitor Cocktail (4693159001, Sigma-Aldrich) and freeze-thawed 3 times. After spinning down for 30 min at 21.000 x g, the supernatant was diluted with 4 X Laemmli sample buffer supplemented with 2-mercaptoethanol according to the manufacturer's instructions (1610747, Bio-Rad) and denatured at 95°C for 5 min. Proteins were separated using 4–15% Criterion™ TGX™ Precast Midi Protein Gel (5671085, Bio-Rad) and transferred to nitrocellulose membranes using a transfer kit (1704270, Bio-rad). As a loading control beta-actin was used (ab6276, Abcam) and for MTH1, anti-MTH1 (NB100-109, Novus biologicals). Secondary antibodies used were IRDye 680RD Donkey anti-mouse (925-68072, Licor) and IRDye® 800CW Donkey anti-Rabbit (925-32213, Licor). Uncropped western blots are shown in Supplementary Figure S8.

Western Blot H3 p-Ser10 and MTH1 levels 0-24h

Cells were washed with PBS and lysed on ice by re-suspending in 30 μ L lysis buffer (100 mM Tris-HCl pH 8, 150 mM NaCl, 1% NP-40) supplemented with 1x cOmplete® protease inhibitor cocktail (Roche) and 1x Halt® phosphatase inhibitor cocktail (ThermoFisher Scientific).

Samples were incubated on ice for 30 min, sonicated 3x 10 sec at 50 % amplitude and then centrifuged at 25,000 x g for 20 min to remove debris. Protein concentration of cell lysates was quantified by using the Pierce BCA Protein Assay Kit (ThermoFisher Scientific) and samples were adjusted to contain equal amounts of protein. Samples were denatured at 70 °C for 10 min in NuPAGE LDS sample buffer and NuPAGE reducing agent (ThermoFisher Scientific). Proteins were resolved on a 4-15% Mini-PROTEAN® TGX precast gel (Bio-Rad) at 130 V for 1 h. Proteins were transferred to nitrocellulose membranes (Bio-Rad) by using Trans-Blot Turbo Transfer System (Bio-Rad). Membranes were blocked for 1 h at room temperature in blocking buffer (5 % milk in 25 mM Tris, 0.15 M NaCl, 0.05 % Tween-20, pH 7.5 (TBS-T)) and incubated in primary antibody solutions under rotation at 4° C overnight. The following primary antibodies were used: rabbit anti-MTH1 (Novus Biologicals, cat. no. NB100-109, 1:500), rabbit anti-H3 p-Ser10 (Abcam, cat. no. ab5176, 1:500) and mouse anti- β -actin (Abcam, cat. no. ab6276, 1:10,000). Thereafter, membranes were washed three times in TBS-T and incubated with IRDye® 800CW secondary antibody diluted in 5 % milk blocking buffer at room temperature for 1 h. The secondary antibodies used were donkey anti-rabbit IRDye 800CW (926-32213, 1:5,000) and donkey anti-mouse IRDye 800CW (cat. no. 926-32212, 1:5,000) from Li-Cor Biosciences. Protein bands were visualized using an Odyssey® Fc imager (LI-COR Biosciences) and quantified using ImageJ software. Uncropped western blots are shown in Supplementary Figure S8.

CellROX redox assay

T cells were activated on subsequent days (Fig. 1A) in 96 well plates (0.8 million/mL, 200 μ L) and treated at the same time with TH1579. On the harvest day, control wells were first pre-incubated with 400 μ M tert-butyl hydroperoxide (TBHP) or 5 mM N-acetyl cysteine as

technical controls for 1h (only TBHP shown in Fig. 1E). CellROX™ Green Reagent (C10444, Thermo Fisher Scientific) was then added to the medium in the wells at a ratio of 1:500 for 30 min. For washing, cells were first held over a 96-well plate magnet to remove the activation beads by pipetting, and then an equal volume from each well was transferred to a conical bottom 96 well plate (249935, Thermo Fisher Scientific) into which 10 µL of counting beads for flow cytometry (424902, Biolegend) had been pre-pipetted. Cells were washed with 4 °C phosphate buffered saline (PBS) and incubated for 30 min 1:1000 with the fixable viability dye LIVE/DEAD™ Fixable Yellow Dead Cell Stain Kit (L34967, Thermo Fisher Scientific) at 4 °C. Cells were washed and fixed in 4% paraformaldehyde solution (sc-281692, Santa Cruz Bio) for 15 min. Fixed cells were washed and permeabilized in CellWASH (349524, Becton Dickinson) containing 2% BSA and 0.1 % Saponin, and incubated at RT for 30 min. Permeabilized cells were stained with anti MTH1 (NB100-109, Novus biologicals) at 1:500 at RT for 30 min, washed and stained with secondary Alexa Fluor (AF) 647 antibody (A-31573, Invitrogen) for 30 min before 2 final washes and dilution in FBS-free CellWASH. Only live cells were analyzed, after discriminating for cells of proper Forward/side scatter (FSC/SSC), single cells and negative Live/dead. Relative cell count was determined as live cells per total counting beads, for each sample, compared to the mean of the DMSO control.

MTH1 levels per cell generation

Enriched T cells were stained with 1:1000 CFSE CellTrace (C34554, Thermo Fisher Scientific) in PBS, according to the manufacturer's instructions. Cells were then activated and treated simultaneously (0.8 million/mL, 1.25 mL) and cultured for 96h in 12-well plates (83.3921.500, Sarstedt). Dynabeads were removed and cells were incubated with LIVE/DEAD™ Fixable Yellow Dead Cell Stain Kit, prior to fixing with eBioscience™

Transcription Factor Staining Buffer Set (00-5523-00, Thermo Fisher Scientific) following the manufacturer's instructions. Cells were then permeabilized with saponin and stained for MTH1 as described above, and finally stained for CD4 APC-H7 (560158, Becton Dickinson) and CD8 APC (561421, Becton Dickinson) for 30 min, before washed with PBS. Single cells were gated for, and from them only LIVE/DEAD™ -negative cells were investigated, to exclude dead cells. The generations were determined using the automatic cell generation tracker in FlowJo.

Flow cytometry of H3 p-Ser10 and cell cycle

Enriched T cells were activated for 96h and then treated with inhibitor for 24 h. Cells were then fixed in 4% paraformaldehyde solution and permeabilized with 0.1% Saponin solution as described above. Cells were then stained with rabbit anti-H3 p-Ser10 (Abcam, cat. no. ab5176, 1:100) for 30 min at RT for 30 min, then washed and incubated with secondary antibody Alexa Fluor (AF) 647 antibody (A-31573, Invitrogen). Finally, cells were washed and stained with 1 µg/mL PI (P4170 , Sigma Aldrich). Single cells were determined by both FSC-height vs. FSC-area, and PI-height vs. PI-area.

Apoptosis and CD71 expression

Enriched CD3+ T cells were activated for 96 h and then treated with compound for up to an additional 96h. Cells were stained for CD3 PE-Cy7 (563423, Becton Dickinson), CD4 APC-H7 (560158, Becton Dickinson), CD8 PE (555367, Becton Dickinson) and CD71 APC or BV786 (334108, Nordic Biosite or 563768, Becton Dickinson) for 30 min at 4°C, following wash with CellWASH and addition of Sytox blue (S34857, Thermo Fisher Scientific) and Annexin V FITC (556420, BD) in Annexin binding buffer (422201, Nordic biosite) for 15 min before analysis.

Single cells were gated for CD3+ or CD3+CD4+ and CD3+CD8+ and then plotted against Sytox blue and Annexin V. Double negative were considered live, Annexin+Sytox- early apoptotic, Annexin+Sytox+ late apoptotic and Annexin-Sytox+ necrotic. Among the live cells, the median fluorescence intensity (MFI) of CD71 was measured.

Cell cycle and γ H2AX

Enriched T cells were activated for 96h, followed by labelling with 10 μ M EdU (CLK-N001-100, Jena Bioscience) for 30 min in medium at 37°C. Cells were then washed and treated with inhibitor for 4h or 24h. For cell harvest, cells were fixed in 4% PFA and permeabilized with Saponin as described above. A click reaction was performed using 800 μ M CuSO₄, 5mM ascorbic acid (A4403, Sigma-Aldrich) and 0.5 μ M Atto 488 azide (AD 488-101, Atto-tec) in PBS with 0.2% BSA and 0.1% saponin for 30 min at RT. Cells were then incubated with anti- γ H2AX AF-647 (613407, Nordic Biosite) for 30 min followed by washing and resuspension in 0.2% BSA 0.1% Saponin PBS with DAPI (D1306, Thermo Fisher Scientific) and a 15 min incubation at RT before analysis. Single cells were discriminated by using FSC-area vs. FSC-height, and DAPI-area vs. DAPI-height. The DMSO control was used in addition to the FMO control to set the gate for γ H2AX positivity, and cell cycle phase was determined based on the histogram of DAPI, either all cells or EdU positive or negative (Fig. 3B).

mRNA and RT-qPCR

Harvested T cells were lysed in TRIzol™ reagent (15596026, Thermo Fisher Scientific) and mRNA was purified using the Direct-zol™ RNA MiniPrep w/ Zymo-Spin™ IIC Columns (R2052, Nordic Biosite). cDNA was then generated using Quanti tect Reverse Transcription Kit (205314, Qiagen) and RT-qPCR was performed using Luminaris Color HiGreen qPCR Master

Mix (K0393, Thermo Fisher Scientific) in a Rotorgene (Qiagen, Venlo, Netherlands), and quantified using the $2^{-\Delta\Delta CT}$ method with β -actin as housekeeping gene. The primers used were as follows:

MTH1_Foward: GTGCAGAACCCAGGGACCAT

MTH1_Reverse: GCCCACGAACTCAAACACGA

β -Actin_Foward: CCTGGCACCCAGCACAAT

β -Actin_Reverse: GGGCCGGACTCGTCATACT

Resazurin assay

Cells were activated for 96 h. After, 20-40 000 cells per well were seeded into 384 well plates (CLS3764-100EA, Corning) pre-spotted with compound. The cells were incubated for 96 h, followed by addition of Resazurin at a final concentration of 10 μ g/mL and an additional incubation of 6 h. The fluorescence (544/595nm) was measured using a microplate reader (Hidex Sense). As normalization controls, DMSO samples (100 %) and wells with only media (0 %) were used.

COMET assay

200 000 activated T cells were seeded into 6-well plates. The next day cells were treated with DMSO or MTH1 inhibitors for 24 h. Cells were then harvested by trypsinization and washed with 1X cold PBS, re-suspended in 1X cold PBS at a concentration of about 1 million cells/ml. Later, the cell suspension was mixed with 1.2 % low melting agarose and was layered over 1% agarose coated fully frosted slides. The slides were incubated in lysis buffer containing [100 mmol/L sodium EDTA, 2.5 mol/L NaCl, 10 mmol/L Tris-HCl (pH 10)], 1% Triton X-100 and 10% DMSO at 4°C in the dark overnight. Slides were washed 3 times with

enzyme buffer containing Hepes, KCl, EDTA, followed by addition of OGG1 enzyme and incubated at 37°C for 45 min. At the end of the incubation period, alkaline denaturation with alkali buffer (300 mmol/L NaOH, 1 mmol/L sodium EDTA) was carried out in an electrophoresis chamber for 20 min. Electrophoresis was run at 25 V and 300 mA in the same buffer for 30 min. The slides were later neutralized with neutralizing buffer [250 mmol/L Tris-HCl (pH 7.5)] for 45 min. Just before imaging, the slides were stained with 1X SYBR gold dye (S11494, Thermo Fisher Scientific). Images were taken using a confocal microscope (LSM 780, Zeiss) with a 20X objective and analysis was performed using CometScore software.

EAE model

Female C57BL/6 mice were purchased from Taconic (Lille Skensved, Denmark) and maintained in an animal facility at Karolinska Hospital. All mice were between 9 and 11 weeks of age, weighing 20–23g, were pathogen-free, and had access to chow and water *ad libitum*. All experiments performed were in accordance with the local ethical committee in Stockholm North, number N138/14. Recombinant protein corresponding to the N-terminal sequence of mouse MOG (amino acids 1–125) was expressed in *Escherichia coli* and purified to homogeneity by chelate chromatography. Purified MOG dissolved in 6 M urea was dialyzed against sodium acetate buffer (10 mM, pH 3.0) to obtain a soluble preparation that was stored frozen at -20 °C. Mice were anesthetized with isoflurane (Forane; Abbott Laboratories, Abbot Park, IL) and injected subcutaneously at the dorsal tail base with 100 µL inoculum containing 50 µg of MOG in phosphate-buffered saline (PBS) emulsified in Complete Freund's Adjuvant (CFA) containing 100 µg heat-killed *Mycobacterium tuberculosis* H37Ra (Difco Laboratory, Detroit, MI). All immunized mice were treated either

with TH1579 solution at a dose of 5 mg/kg or with control solution twice per day for consecutive 6 days by gavage. The mice were randomly divided into 3 treatment groups: control group (n = 8), TH1579 treatment group starting from day 1 post-immunization (p.i) (n = 8), and TH1579 treated group starting from day 12 p.i. (n = 7). In other repetitions where only the control group and the group with TH1579 from day 1 were analyzed, n = 7-8 per group. Mice were weighed and scored daily for clinical signs of EAE using a 6-point scale as follows: 0, no clinical signs of EAE; 1, tail weakness or tail paralysis; 2, hindlimb paraparesis or hemiparesis; 3, hindlimb paralysis or hemiparalysis; 4, tetraplegia or moribund; and 5, death.

Preparation of single cell suspensions from spleens and lymph nodes of EAE mice

On day 23 p.i. the mice from the control group (n = 7 and 8 in 2 separate experiments) and the day 1 p.i. TH1579 treated group (n = 7 and 8 in 2 separate experiments) were sacrificed and spleens were dissected. Splenocytes were obtained by mechanically disrupting spleens through a 40 µm nylon strainer. Erythrocytes were lysed using ACK buffer (Gibco) for 5 min on ice and washed with D-PBS. Splenocytes were cultured in anti-CD3 and anti-CD28 molecular complex (Becton Dickinson)-coated 96-well flat-bottom plates (Corning) for 48 h, with stimulation of MOG (10 µg/mL) or ConA (5 µg/mL). Proliferation was measured using [methyl-3H]thymidine (Amersham, Aylesbury, UK) at a concentration of 1 mCi/well.

In a separate experiment, immunized mice were treated with TH1579 solution at a dose of 5 mg/kg subcutaneously, either once per day or twice per day, starting from day 1 for 6 consecutive days, and then sacrificed to dissect inguinal lymph nodes at day 7 p.i. with MOG. Two animals per group were used. The single cell suspensions were prepared from lymph

nodes and incubated with the following antibodies for flow cytometric analysis: FITC-CD4 (clone: RM4-5, BD Biosciences), PE-CD8 (clone: 53-6.7, eBioscience), Percp-Cy5.5-CD3 (clone: 145-2C11, BioLegend), APC-CD62L (clone: MEL-14, eBioscience), Alexa Fluor700-CD44 (clone: IM7, BioLegend). Cells were acquired using a Gallios flow cytometer (Beckman Coulter, Brea, CA, United States) and analyzed using Kaluza software (Beckman Coulter, Brea, CA, United States).

Toxicity studies on other immune cells

Heparinized whole venous blood from healthy human donors was used. Three to four donors were used for every test system applied. Male and female donors, age 30-60, participated in the study. All samples were anonymized pre-testing. General cytotoxicity of the test compound was investigated by flow cytometric analysis of PBMC and K562-cells exposed to 2-20 μ M test compound overnight and for 4 hours, respectively, at 37°C and 5% CO₂.

Phagocytosis: Prior to experimental start, heparinized human whole blood was cooled in an ice-water bath for 10 min. 100 μ L samples of blood were then transferred to test tubes with non-toxic concentrations of the test compound or the corresponding amount of DMSO, using duplicate cultures. The tubes were incubated for 30 min at 37°C. FITC-labelled opsonized *E. coli* were then added and the tubes were incubated for another 10 minutes at 37°C. Tubes incubated at 37°C, not exposed to any compound, served as positive controls, while tubes incubated at 4°C served as negative controls. After incubation, RBCs were lysed, the samples fixed and washed once, and propidium iodide (PI) was added for labeling of eukaryotic cells to enable gating for flow cytometry.

Oxidative burst: Prior to experimental start, heparinized human whole blood was cooled in an ice-water bath for 10 min. 100 μ L samples of blood were then transferred to test tubes with non-toxic concentrations of the test and reference compounds, using duplicate cultures. The tubes were incubated for 30 min at 37°C. Opsonized *E. coli* were added and the tubes incubated for another 10 minutes at 37°C. Tubes incubated at 37°C, not exposed to any compound, served as positive controls while tubes incubated without *E. coli* were used as negative controls. After incubation, the substrate solution dihydrorhodamine was added to all tubes, followed by incubation at 37°C for another 10 min. After this final incubation, RBCs were lysed, the cells fixed and washed once, and PI was added for labeling of eukaryotic cells to enable gating for flow cytometry. The reference compound for suppression of oxidative burst was Apocynin (A-10809, Sigma) at 92 μ g/mL and 31 μ g/mL.

For phagocytosis and oxidative burst, data was collected using a Flow-cytometer type FACSCantoll (Becton Dickinson, Franklin Lakes, NJ, United States). A live gate was set on red fluorescence to collect diploid cells (exclusion of bacteria). 10 000 events from each sample were collected. Live-gated cells were further exposed in a green-fluorescence histogram for determination of proportion of positive cells (given in %) and MFI, respectively. Monocytes and granulocytes were analyzed separately.

NK cell cytotoxicity: Effector cells (E), lymphoid cells isolated from human peripheral blood, were pre-incubated for 1 hour with test substance or reference compound with or without IL-2. Effector cells pre-incubated without test substance served as a positive control for donor-specific background of NK-cytotoxicity. CFSE-labeled human K562-cells (human

erythromyeloblastoid leukemia cell line) served as target cells (T). Following pre-incubation of effector cells with test- or reference substance, E and T were mixed at a 50:1 or 100:1 ratio with reference to total% NK-cells detected in the lymphoid cell population of each donor. After vortexing, the cells were spun down at 120 x g, 2 minutes. The tubes were then put in a 37°C water bath placed in a cell incubator for approx. 4 h at 37°C and 5% CO₂. Target cells incubated with or without test substance were used as a control for the frequency of spontaneously dead cells. After incubation, the samples were put in an ice water bath and PI was added for DNA staining of permeabilized/dead target cells. The samples were incubated for 5 minutes and measured using a flow cytometer within 60 minutes after PI addition. Doxycycline (D-3447, Sigma) was used as reference compound for inhibition of NK-cytotoxicity at 50 and 25 µg/mL test concentrations, respectively.

Immunization studies in rats; TDAR (T-cell Dependent Antibody Response)

The study was designed according to ICH S8 - Immunotoxicity Studies for Human Pharmaceuticals and performed at former Swetox, Karolinska Institute, Sweden. The ethical license number is S7-15. The animals used were 64 female rats of approximately 10 weeks (RccHan: Wistar Rat, Envigo, Venray, Netherlands), divided into 8 groups of 8 animals each. Animals were ordered based on weights and ages within a narrow limit, and randomized by putting batches of 2 or 3 females in group cages in the order they arrived to the test facility. An overview of the study is presented in Fig. 7G. The first day of dosing was designated *Day 1* and the first seven days as *Week 1*. The week prior to dosing was designated as *Week -1*. TH1579 was administered orally by gavage. All animals were given TH1579 (or vehicle) twice daily, every second day, between Days 1-33. Immunization was performed during the dosing period (Days 1-33) in Groups 1 to 4, and during a similar dose-free period following an

approximately 4-week recovery period in Groups 5 to 8. The test article for immunization was Imject® Mariculture KLH in phosphate buffered saline (PBS) solution (Pierce, Product No. 77600, Batch RE234729). The formulation with KLH was administered intravenously, 300 µg/animal, via the tail vein, as an i.v infusion on days 15 and 29 (groups 1-4) and on days 65 and 79 (groups 5-8) to create primary and a secondary IgM- and IgG responses, respectively. The doses of TH1579 used were 2 x 3.3 mg/kg/dosing day for groups 2 and 6; 2 x 10 mg/kg/dosing day for groups 3 and 7; 2 x 30 mg/kg/dosing day for groups 4 and 8.

The general condition of all animals was assessed daily. All animals were thoroughly examined after arrival and before the first day of dosing. In case of clinical symptoms more than 15 minutes after dose, animals were checked occasionally and the approximate time of recovery from observed symptoms was noted. Animals were observed at least once during each time interval 0-3, 3-6 and 6-24 hours after dosing.

Blood samples for hematology: Blood for scheduled hematology was taken at *Week -1*, (Groups 1-8), that is before dosing and immunization, from a peripheral vein in capillary EDTA tubes, and additionally on Day 35 (Groups 1-4 at necropsy) and for groups 5-8 in the week before immunization on Day 65 and on Day 85 at necropsy. Blood was analyzed using an Exigo analyzer by the Responsible technician for Clinical Pathology at Swetox, Sweden.

Blood samples for antibody analysis: Individual blood samples were taken from a peripheral vein prior to dose with TH1579 (all groups), Days 15, 20, 29 and 34 (group 1-4, prior to injection with KLH), Days 65, 70, 79 and 84, and at the end of study (group 5-8, prior to injection with KLH). The concentrations of anti-KLH IgG and IgM were determined by ELISA.

Supplementary information is available at Cell Death & Differentiation's website

REFERENCES

1. Hayter SM, Cook MC. Updated assessment of the prevalence, spectrum and case definition of autoimmune disease. *Autoimmun Rev.* 2012;11(10):754-65.
2. Rosenblum MD, Gratz IK, Paw JS, Abbas AK. Treating human autoimmunity: current practice and future prospects. *Sci Transl Med.* 2012;4(125):125sr1.
3. Wang L, Wang FS, Gershwin ME. Human autoimmune diseases: a comprehensive update. *J Intern Med.* 2015;278(4):369-95.
4. Bluestone JA, Bour-Jordan H, Cheng M, Anderson M. T cells in the control of organ-specific autoimmunity. *Journal of Clinical Investigation.* 2015;125(6):2250-60.
5. Raphael I, Nalawade S, Eagar TN, Forsthuber TG. T cell subsets and their signature cytokines in autoimmune and inflammatory diseases. *Cytokine.* 2015;74(1):5-17.
6. Goodnow CC, Sprent J, Fazekas de St Groth B, Vinuesa CG. Cellular and genetic mechanisms of self tolerance and autoimmunity. *Nature.* 2005;435(7042):590-7.
7. Li P, Zheng Y, Chen X. Drugs for Autoimmune Inflammatory Diseases: From Small Molecule Compounds to Anti-TNF Biologics. *Front Pharmacol.* 2017;8:460.
8. Sarzi-Puttini P, Ceribelli A, Marotto D, Batticciotto A, Atzeni F. Systemic rheumatic diseases: From biological agents to small molecules. *Autoimmun Rev.* 2019;18(6):583-92.
9. Monaco C, Nanchahal J, Taylor P, Feldmann M. Anti-TNF therapy: past, present and future. *International immunology.* 2014;27(1):55-62.
10. Wang W, Zhou H, Liu L. Side effects of methotrexate therapy for rheumatoid arthritis: A systematic review. *European journal of medicinal chemistry.* 2018;158:502-16.
11. Mazaud C, Fardet L. Relative risk of and determinants for adverse events of methotrexate prescribed at a low dose: a systematic review and meta-analysis of randomized placebo-controlled trials. *British journal of dermatology (1951).* 2017;177(4):978-86.
12. Quezada SM, McLean LP, Cross RK. Adverse events in IBD therapy: the 2018 update. *Expert review of gastroenterology & hepatology.* 2018;12(12):1183-91.
13. Grulich AE, van Leeuwen MT, Falster MO, Vajdic CM. Incidence of cancers in people with HIV/AIDS compared with immunosuppressed transplant recipients: a meta-analysis. *Lancet.* 2007;370(9581):59-67.
14. Nathan C, Cunningham-Bussell A. Beyond oxidative stress: an immunologist's guide to reactive oxygen species. *Nat Rev Immunol.* 2013;13(5):349-61.
15. Franchina DG, Dostert C, Brenner D. Reactive Oxygen Species: Involvement in T Cell Signaling and Metabolism. *Trends Immunol.* 2018;39(6):489-502.
16. Belikov AV, Schraven B, Simeoni L. T cells and reactive oxygen species. *J Biomed Sci.* 2015;22:85.
17. Simeoni L, Bogeski I. Redox regulation of T-cell receptor signaling. *Biological Chemistry* 2015. p. 555.
18. Previte DM, O'Connor EC, Novak EA, Martins CP, Mollen KP, Piganelli JD. Reactive oxygen species are required for driving efficient and sustained aerobic glycolysis during CD4(+) T cell activation. *Plos One.* 2017;12(4).
19. Buck MD, O'Sullivan D, Geltink RIK, Curtis JD, Chang CH, Sanin DE, et al. Mitochondrial Dynamics Controls T Cell Fate through Metabolic Programming. *Cell.* 2016;166(1):63-76.
20. Pearce EL, Poffenberger MC, Chang CH, Jones RG. Fueling immunity: insights into metabolism and lymphocyte function. *Science.* 2013;342(6155):1242454.

21. MacIver NJ, Michalek RD, Rathmell JC. Metabolic regulation of T lymphocytes. *Annu Rev Immunol.* 2013;31:259-83.
22. Moloney JN, Cotter TG. ROS signalling in the biology of cancer. *Seminars in Cell & Developmental Biology.* 2018;80:50-64.
23. Hanahan D, Weinberg RA. Hallmarks of cancer: the next generation. *Cell.* 2011;144(5):646-74.
24. Cassim S, Vucetic M, Zdravlevic M, Pouyssegur J. Warburg and Beyond: The Power of Mitochondrial Metabolism to Collaborate or Replace Fermentative Glycolysis in Cancer. *Cancers.* 2020;12(5).
25. Luo M, He H, Kelley MR, Georgiadis MM. Redox regulation of DNA repair: implications for human health and cancer therapeutic development. *Antioxidants & redox signaling.* 2010;12(11):1247-69.
26. Sakumi K, Furuichi M, Tsuzuki T, Kakuma T, Kawabata S, Maki H, et al. Cloning and expression of cDNA for a human enzyme that hydrolyzes 8-oxo-dGTP, a mutagenic substrate for DNA synthesis. *Journal of Biological Chemistry.* 1993;268(31):23524.
27. Oka S, Ohno M, Tsuchimoto D, Sakumi K, Furuichi M, Nakabeppu Y. Two distinct pathways of cell death triggered by oxidative damage to nuclear and mitochondrial DNAs. *The EMBO journal.* 2008;27(2):421-32.
28. Ichikawa J, Tsuchimoto D, Oka S, Ohno M, Furuichi M, Sakumi K, et al. Oxidation of mitochondrial deoxynucleotide pools by exposure to sodium nitroprusside induces cell death. *DNA repair.* 2008;7(3):418-30.
29. Carter M, Jemth A-S, Hagenkort A, Page BDG, Gustafsson R, Griese JJ, et al. Crystal structure, biochemical and cellular activities demonstrate separate functions of MTH1 and MTH2. *Nature communications.* 2015;6(1):7871-.
30. Teruhisa T, Akinori E, Hisato I, Tomoo I, Yoko N, Yohei T, et al. Spontaneous Tumorigenesis in Mice Defective in the MTH1 Gene Encoding 8-Oxo-dGTPase. *Proceedings of the National Academy of Sciences - PNAS.* 2001;98(20):11456-61.
31. Oda H, Nakabeppu Y, Furuichi M, Sekiguchi M. Regulation of expression of the human MTH1 gene encoding 8-oxo-dGTPase. Alternative splicing of transcription products. *J Biol Chem.* 1997;272(28):17843-50.
32. Gad H, Koolmeister T, Jemth AS, Eshtad S, Jacques SA, Strom CE, et al. MTH1 inhibition eradicates cancer by preventing sanitation of the dNTP pool. *Nature.* 2014;508(7495):215-21.
33. Warpmann Berglund U, Sanjiv K, Gad H, Kalderen C, Koolmeister T, Pham T, et al. Validation and development of MTH1 inhibitors for treatment of cancer. *Ann Oncol.* 2016;27(12):2275-83.
34. Hua XW, Sanjiv K, Gad H, Pham T, Gokturk C, Rasti A, et al. Karonudib is a promising anticancer therapy in hepatocellular carcinoma. *Therapeutic Advances in Medical Oncology.* 2019;11.
35. Magkouta SF, Pappas AG, Vaitis PC, Agioutantis PC, Pateras IS, Moschos CA, et al. MTH1 favors mesothelioma progression and mediates paracrine rescue of bystander endothelium from oxidative damage. *JCI insight.* 2020;5(12).
36. Brautigam L, Pudenko L, Jemth AS, Gad H, Narwal M, Gustafsson R, et al. Hypoxic Signaling and the Cellular Redox Tumor Environment Determine Sensitivity to MTH1 Inhibition. *Cancer Res.* 2016;76(8):2366-75.
37. Hirahara K, Nakayama T. CD4⁺ T-cell subsets in inflammatory diseases: beyond the Th1/Th2 paradigm. *International immunology.* 2016;28(4):163-71.

38. Zhu J. T Helper Cell Differentiation, Heterogeneity, and Plasticity. Cold Spring Harbor perspectives in biology. 2018;10(10):a030338.
39. Gad H, Mortusewicz O, Rudd SG, Stolz A, Amaral N, Brautigham L, et al. MTH1 promotes mitotic progression to avoid oxidative DNA damage in cancer cells. bioRxiv. 2019.
40. Rudd SG, Gad H, Sanjiv K, Amaral N, Hagenkort A, Groth P, et al. MTH1 Inhibitor TH588 Disturbs Mitotic Progression and Induces Mitosis-Dependent Accumulation of Genomic 8-oxodG. Cancer research (Chicago, Ill). 2020;80(17):3530-41.
41. Bivik Eding C, Köhler I, Verma D, Sjögren F, Bamberg C, Karsten S, et al. MTH1 Inhibitors for the Treatment of Psoriasis. Journal of investigative dermatology. 2021.
42. Samaranayake GJ, Troccoli CI, Zhang L, Mai H, Jayaraj CJ, Ji D, et al. The Existence of MTH1-independent 8-oxodGTPase Activity in Cancer Cells as a Compensatory Mechanism against On-target Effects of MTH1 Inhibitors. Molecular cancer therapeutics. 2020;19(2):432-46.
43. Zhu J, Yamane H, Paul WE. Differentiation of effector CD4 T cell populations (*). Annu Rev Immunol. 2010;28:445-89.
44. Loo TT, Gao Y, Lazarevic V. Transcriptional regulation of CD4(+) TH cells that mediate tissue inflammation. J Leukoc Biol. 2018;104(6):1069-85.
45. O'Garra A. Cytokines induce the development of functionally heterogeneous T helper cell subsets. Immunity. 1998;8(3):275-83.
46. Abimannan T, Peroumal D, Parida JR, Barik PK, Padhan P, Devadas S. Oxidative stress modulates the cytokine response of differentiated Th17 and Th1 cells. Free Radic Biol Med. 2016;99:352-63.
47. Chapman NM, Boothby MR, Chi H. Metabolic coordination of T cell quiescence and activation. Nature reviews Immunology. 2019;20(1):55-70.
48. Leone RD, Powell JD. Metabolism of immune cells in cancer. Nature reviews Cancer. 2020;20(9):516-31.
49. Tse HM, Thayer TC, Steele C, Cuda CM, Morel L, Piganelli JD, et al. NADPH oxidase deficiency regulates Th lineage commitment and modulates autoimmunity. J Immunol. 2010;185(9):5247-58.
50. Previte DM, Piganelli JD. Reactive Oxygen Species and Their Implications on CD4(+) T Cells in Type 1 Diabetes. Antioxidants & Redox Signaling. 2018;29(14):1399-414.
51. Kimura K. Regulatory T cells in multiple sclerosis. Clinical & experimental neuroimmunology. 2020;11(3):148-55.
52. Erdman SE, Poutahidis T, Tomczak M, Rogers AB, Cormier K, Plank B, et al. CD4 + CD25 + Regulatory T Lymphocytes Inhibit Microbially Induced Colon Cancer in Rag2-Deficient Mice. The American journal of pathology. 2003;162(2):691-702.
53. Cooke MS, Evans MD, Dizdaroglu M, Lunec J. Oxidative DNA damage: mechanisms, mutation, and disease. Faseb Journal. 2003;17(10):1195-214.
54. Lu R, Nash HM, Verdine GL. A mammalian DNA repair enzyme that excises oxidatively damaged guanines maps to a locus frequently lost in lung cancer. Current biology. 1997;7(6):397-407.
55. Hazra TK, Hill JW, Izumi T, Mitra S. Multiple DNA glycosylases for repair of 8-oxoguanine and their potential in Vivo functions. Progress in Nucleic Acid Research and Molecular Biology. 2001;68:193-205.
56. German P, Szaniszló P, Hajas G, Radak Z, Bacsi A, Hazra TK, et al. Activation of cellular signaling by 8-oxoguanine DNA glycosylase-1-initiated DNA base excision repair. DNA repair. 2013;12(10):856-63.

57. Mabley JG, Pacher P, Deb A, Wallace R, Elder RH, Szabo C. Potential role for 8-oxoguanine DNA glycosylase in regulating inflammation. *FASEB J.* 2005;19(2):290-2.
58. Touati E, Michel V, Thiberge J-M, Ave P, Huerre M, Bourgade F, et al. Deficiency in OGG1 Protects against Inflammation and Mutagenic Effects Associated with *H. pylori* Infection in Mouse. *Helicobacter* (Cambridge, Mass). 2006;11(5):494-505.
59. Li GP, Yuan KF, Yan CG, Fox J, Gaid M, Breitwieser W, et al. 8-Oxoguanine-DNA glycosylase 1 deficiency modifies allergic airway inflammation by regulating STAT6 and IL-4 in cells and in mice. *Free Radical Biology and Medicine.* 2012;52(2):392-401.
60. Bacsı A, Aguilera-Aguirre L, Szczesny B, Radak Z, Hazra TK, Sur S, et al. Down-regulation of 8-oxoguanine DNA glycosylase 1 expression in the airway epithelium ameliorates allergic lung inflammation. *DNA Repair.* 2013;12(1):18-26.
61. Ba X, Aguilera-Aguirre L, Rashid QTAN, Bacsı A, Radak Z, Sur S, et al. The role of 8-oxoguanine DNA glycosylase-1 in inflammation. *International journal of molecular sciences.* 2014;15(9):16975-97.
62. Visnes T, Cazares-Korner A, Hao WJ, Wallner O, Masuyer G, Loseva O, et al. Small-molecule inhibitor of OGG1 suppresses proinflammatory gene expression and inflammation. *Science.* 2018;362(6416):834-+.
63. Qin S, Lin P, Wu Q, Pu Q, Zhou C, Wang B, et al. Small-Molecule Inhibitor of 8-Oxoguanine DNA Glycosylase 1 Regulates Inflammatory Responses during *Pseudomonas aeruginosa* Infection. *The Journal of immunology* (1950). 2020;205(8):ji1901533-2242.
64. Stratigopoulou M, van Dam TP, Guikema JEJ. Base Excision Repair in the Immune System: Small DNA Lesions With Big Consequences. *Frontiers in immunology.* 2020;11:1084-.
65. Pazzaglia S, Pioli C. Multifaceted Role of PARP-1 in DNA Repair and Inflammation: Pathological and Therapeutic Implications in Cancer and Non-Cancer Diseases. *Cells* (Basel, Switzerland). 2019;9(1):41.
66. Pateras IS, Havaki S, Nikitopoulou X, Vougas K, Townsend PA, Panayiotidis MI, et al. The DNA damage response and immune signaling alliance: Is it good or bad? Nature decides when and where. *Pharmacol Ther.* 2015;154:36-56.
67. Nakad R, Schumacher B. DNA Damage Response and Immune Defense: Links and Mechanisms. *Front Genet.* 2016;7:147.
68. Kay J, Thadhani E, Samson L, Engelward B. Inflammation-induced DNA damage, mutations and cancer. *DNA repair.* 2019;83:102673-.
69. Bhattacharya S, Srinivasan K, Abdisalaam S, Su F, Raj P, Dozmorov I, et al. RAD51 interconnects between DNA replication, DNA repair and immunity. *Nucleic acids research.* 2017;45(8):4590-605.
70. Sahraian MA, Soltani BM, Behmanesh M. Alteration of OGG1, MYH and MTH1 genes expression in relapsing-remitting multiple sclerosis patients. *PHYSIOLOGY AND PHARMACOLOGY.* 2017;21(2):129-36.
71. Kumagae Y, Hirahashi M, Takizawa K, Yamamoto H, Gushima M, Esaki M, et al. Overexpression of MTH1 and OGG1 proteins in ulcerative colitis-associated carcinogenesis. *Oncol Lett.* 2018;16(2):1765-76.
72. Sakumi K, Tominaga Y, Furuichi M, Xu P, Tsuzuki T, Sekiguchi M, et al. Ogg1 knockout-associated lung tumorigenesis and its suppression by Mth1 gene disruption. *Cancer research* (Chicago, Ill). 2003;63(5):902-5.
73. Karran P, Attard N. Thiopurines in current medical practice: molecular mechanisms and contributions to therapy-related cancer. *Nature reviews Cancer.* 2008;8(1):24-36.

74. Sintchak MD, Fleming MA, Futer O, Raybuck SA, Chambers SP, Caron PR, et al. Structure and Mechanism of Inosine Monophosphate Dehydrogenase in Complex with the Immunosuppressant Mycophenolic Acid. *Cell (Cambridge)*. 1996;85(6):921-30.
75. Al-Badr AA, Ajarim TDS. Ganciclovir. Profiles of drug substances, excipients, and related methodology. 2018;43:1-208.
76. Beck S, Zhu Z, Oliveira MF, Smith DM, Rich JN, Bernatchez JA, et al. Mechanism of Action of Methotrexate Against Zika Virus. *Viruses*. 2019;11(4):338.
77. Einarsdottir BO, Karlsson J, Soderberg EMV, Lindberg MF, Funck-Brentano E, Jespersen H, et al. A patient-derived xenograft pre-clinical trial reveals treatment responses and a resistance mechanism to karonudib in metastatic melanoma. *Cell Death Dis*. 2018;9(8):810.
78. Filippi M, Bar-Or A, Piehl F, Preziosa P, Solari A, Vukusic S, et al. Multiple sclerosis. *Nat Rev Dis Primers*. 2018;4(1):43.
79. Dendrou CA, Fugger L, Friese MA. Immunopathology of multiple sclerosis. *Nat Rev Immunol*. 2015;15(9):545-58.

ACKNOWLEDGEMENTS

We thank our chemists Martin Scobie, Tobias Koolmeister, Olov Wallner and Martin Henriksson for all the work on the chemistry side, not the least synthesizing the MTH1 inhibitors. We thank Nadilly Bonagas and Aleksandra Pettke for valuable methodological input and all the members of the Helleday laboratory for discussion and support. We thank Weng-Onn Lui at the flow cytometry lab of the Department of Oncology-Pathology for technical assistance and support.

CONFLICT OF INTEREST STATEMENT

A patent has been filed with data generated in this manuscript, where T.H. is listed as one of the inventors. The patent is fully owned by a non-profit public foundation, the Helleday Foundation for medical research (THF), and T.H. and U.W.B. are members of THF board. Oxcia AB has license to the patent and responsible for clinical development of TH1579. UWB is CEO of Oxcia AB, TH is board member of Oxcia AB. The other authors declare no conflict of interest.

AUTHOR CONTRIBUTION STATEMENT

R.F, S.K., U.W.B. and T.H. devised the concept of the study; U.W.B., R.F., K.C., C.K. and L.B. supervised the project. S.K., R.F., P.M., M.M.S., C.S., K.S, K.C., I.A. and C.K. designed, performed and/or analyzed cell biological experiments. X. Z., R. H., S.K., A. R., T. P., K.C., C.S., B.P., U.W.B. designed, performed and/or analyzed in vivo experiments. S.K. compiled data and prepared the figures; S.K drafted the manuscript supervised by U.W.B, C.K. and T.H; all authors reviewed the final manuscript.

ETHICS STATEMENT

This study was performed in accordance with the Declaration of Helsinki. The *in vitro* experiments on human T cells were performed on products from buffy coats extracted from blood products donated by healthy donors for the blood banks of the Karolinska University Hospital (Stockholm, Sweden), where no additional intervention was performed on the donors specifically for this research. There was no possibility to trace back the samples to the donors.

The *in vivo* studies were approved by the local ethical committees (Stockholm North, number N138/14 for the EAE study; Stockholm South, number S7-15 for the TDAR study).

FUNDING STATEMENT

This work was funded by Karolinska Institute via its CSTP program and research internship program (forskar-AT), The European Research Council (TAROX Programme, ERC-695376, TH), The Swedish Research Council (2015-00162, 2017-06095), and the Torsten and Ragnar Söderberg Foundation (TH).

ABBREVIATIONS

8-oxoG	8-oxo-guanine
AF	Alexa fluor
AZA	Azathioprine
CETSA	Cellular thermal shift assay
CFSE	Carboxyfluorescein
ConA	Concanavalin A
DMSO	Dimethyl sulfoxide
dNMP	Deoxynucleoside monophosphate
dNTP	Deoxynucleoside triphosphate
EAE	Experimental Autoimmune Encephalomyelitis
EdU	5-Ethynyl-2'-deoxyuridine
FMO	Fluorescent minus 1
FSC	Forward scatter
GRAN	Granulocytes
HCT	Hematocrit
HGB	Hemoglobin
KLH	Keyhole limpet hemocyanine
LYM	Lymphocytes
MCH	Mean red cell hemoglobin
MCHC	Mean red cell hemoglobin concentration
MCV	Mean red cell volume
MFI	Median fluorescence intensity
MOG	Myelin oligodendrocyte glycoprotein
MONO	Monocytes
MPV	Mean platelet volume
MS	Multiple sclerosis
MTH1	MutT Homolog 1
MTX	Methotrexate
OGG1	8-Oxoguanine DNA Glycosylase
p.i.	Post immunization
PI	Propidium iodine
PBS	Phosphate buffered saline
PLT	Platelets
RBC	Red blood cells
RDW%	Red cell distribution width (%)
RDWa	Red cell distribution width (absolute)
ROS	Reactive oxygen species
SSC	Side scatter
TBHP	Tert-butyl hydroperoxide
TCR	T cell receptor
WBC	White blood cells

FIGURE LEGENDS

Figure 1: MTH1 is up-regulated in activated human T cells, correlating with an increase in oxidative stress, but the MTH1 increase occurs before the altered redox status is fully detected.

A) Schematic overview of the handling of the T cells in B-I. Human T cells were enriched from Buffy coats of healthy donors and kept in culture stimulated or non-stimulated with CD3/CD28 beads and IL-2 as described in the materials and methods section, for up to 96h.

B-C) Western blot membranes and quantification of stimulated vs. non stimulated T cells after 96h, and relative MTH1 protein levels as compared to non-stimulated cells. Representative images of T cells from 3 different donors. Mean \pm SD shown. The student's t-test was performed for significance[#].

D) Histograms showing the MTH1 levels on single cell level over time in fixed cells, gated for live cells with flow cytometry. 1 representative test sample per time point shown. Experiment performed on T cells from 4 individuals, with minimum 2 replicates each. Dashed line illustrates the positive gate above the fluorescence minus one (FMO) control.

E) Histograms showing the redox level with the redox dye CellROX Green on single cell level over time in fixed cells, gated for live cells with flow cytometry. Tert-butyl hydroperoxide (TBHP) as a technical positive control, in cells pretreated with 400 μ M TBHP for 1h before staining. 1 representative test sample per time point shown. Experiment performed on T cells from 4 individuals, with minimum 2 replicates each. Dashed line illustrates the positive gate above the FMO control.

F) Quantification of flow cytometry plots in G to illustrate the correlation between MTH1 level and oxidative stress in activated human T cells. Graph illustrates the mean of separate experiments with material from 4 donor; One data point is the mean of one individual donor and the combined mean \pm SD is shown. One-way ANOVA as compared to the Resting cells performed for statistical significance[#].

G) Representative flow cytometry plots of F; blue data shows an example sample of resting cells for comparison (same in all consecutive 4 graphs).

H) MTH1 levels in T cells, showing the MTH1 levels among the different cell generation (0-4) after 96h in culture stimulated with CD3/CD28/IL-2. One data point is the mean of one individual donor, and the combined mean \pm SD of the relative MFI compared to the 0-generation for each donor from different experiments is shown.

I) Dot plots of H, illustrating the number of cells in the different generations (density of dots) and consistent MTH1 intensity over the generations as quantified in H. For MTH1 levels in CD4 and CD8 cells, see Fig S2A-B.

#* = $p \leq 0.05$; ** = $p \leq 0.01$; *** = $p \leq 0.001$; **** = $p \leq 0.0001$

Figure 2: MTH1 inhibition is cytotoxic to activated T cells, whereas resting cells are unaffected

A) Cellular Thermal Shift Assay (CETSA) showing an overview of the procedure and target engagement of the MTH1 inhibitor TH1579 in human T cells. All datapoints are normalized to the DMSO control at 37°C. Results from 1 experiment with pooled T cells from 2 individuals are shown, representative of 2 experiments.

B) Schematic overview of the experimental procedure for figure C-H

C) Resazurin assay showing the selectivity of TH1579 for activated T cells, compared with Methotrexate and Azathioprine. Mean + SD shown, 4 technical replicates of 2 individuals per data point, representative of data from at least 6 T cell donors per compound.

D) Survival assay with flow cytometry (Annexin vs. Sytox), showing the effect on CD4 and CD8 human T cells separately after 96h of treatment with different concentrations. Nonlinear fitted curve (line) and single values (dots) as the mean of 3 different individuals of different experiments shown, presented as the relative cell count of live CD3⁺ cells, compared to DMSO (100%). 2-way ANOVA with Šídák's multiple comparisons performed for significance[#], compared to DMSO for the activated CD8 and CD4 cells respectively, and compared to the paired resting controls for each time point.

E) In the same survival assay as D, survival and apoptosis were quantified in resting and activated T cells, here showing the total CD3⁺ cells as illustrated in the dot plots in F. Bar chart shows a representative example of 1 individual with mean + range of 2 data points. For CD4 and CD8 separately, see Fig. S2C.

F) Representative flow cytometry plots from D-E with Annexin-Sytox Blue to the left and the Forward-Side scatter plots to the right, to verify the findings by cell morphology.

G-H) Histogram (G) and bar charts (H) showing the relative median fluorescence intensity of CD71 on the remaining living cells after 96h of treatment, as compared to the DMSO control

(normalized to 1.0). One-way ANOVA compared to the DMSO control performed for significance[#]. For CD4 and CD8 cells separately, see Fig S2D-E.

I) Overview of the experimental procedure in J-K, where the T cells were stimulated and treated with inhibitor simultaneously.

J-K) Histograms (J) and quantifications (K) of cell proliferation using CFSE CellTrace, quantifying the cells left in the original population after 96h of stimulation and treatment. Bar chart in K illustrates the mean of separate experiments with material from 4 donors; 1 data point is the mean of one individual donor and the mean of the different individuals \pm SD is shown. One-way ANOVA performed compared to DMSO for significance[#]. For CD4 and CD8 cells separately, see Fig S2F-G.

[#]* = $p \leq 0.05$; ** = $p \leq 0.01$; *** = $p \leq 0.001$; **** = $p \leq 0.0001$

Figure 3: TH1579 kills T cells by inducing DNA damage in proliferating cells and pushing them towards G2/M arrest.

A) Schematic overview of the experimental procedure in B-G where T cells were activated for 96h, then pulse labelled with EdU and treated with compound for 24h.

B) Dot plots of the T cells and gating strategy for the cell cycle and γ H2AX experiments in C-G, where the EdU positive and negative cells were selected among the already selected single cells.

C) Fraction of all T cells in the different cell cycle phases upon 24h treatment with TH1579. For 4h treatment, see Fig S4B.

D) Fraction the EdU positive cells (SubG1 excluded) in the different cell cycle phases upon 24h treatment with TH1579. For 4h treatment and EdU negative cells, see Fig S4C-B.

E) Dot plots with adjunct histograms of the EdU positive cells (SubG1 excluded) showing γ H2AX against the different cell cycle phases (DAPI). Representative plots from one sample shown. For 4h treatment, EdU negative cells and plots of all cells, see Fig S4A, F.

F) Quantification of % γ H2AX above DMSO control in EdU positive cells (SubG1 excluded), plotted in E, showing the accumulated DNA damage as % γ H2AX positive cells (red rectangle in E) in the different cell cycle phases.

G) Ratio of cells in the different cell cycle phases among the EdU+ γ H2AX+ cells (red rectangle in E).

In A-G, 2-way ANOVA with Šídák's (C-D) or Dunnett's (F-G) multiple comparisons was performed for significance[#]. All experiments were performed on T cells from at least 3 different individuals and the plots show the combined mean \pm SD of different experiments, where 1 data point is the mean of one individual donor.

[#]* = $p \leq 0.05$; ** = $p \leq 0.01$; *** = $p \leq 0.001$; **** = $p \leq 0.0001$.

Figure 4: MTH1 inhibition with TH1579 induces cytotoxicity by mitotic spindle disruption and causes 8-oxoG incorporation.

A-B) Representative dot plots with adjunct histograms (A) and Quantifications (B) for Histone H3 p-Ser10 positive activated T cells treated with TH1579 for 24h (CD3/CD28/IL-2 stimulated for 96h prior to treatment). Representative plots from one sample shown in A). Red gate illustrates the area for Histone H3 p-Ser10 positive cells. Vincristine and resting cells as positive and negative controls, respectively. Absolute values (%) in B, showing the increase upon treatment. Mean \pm SD shown, one-way ANOVA for significance[#]. 1 data point is the mean of one individual donor in a specific experiment.

C-D) Protein quantifications (C) and representative Western blot membrane (D) of Histone H3 p-Ser10 in activated T cells treated with TH1579 for 24h. Relative values normalized to the mean of the DMSO controls of 4 donors. Mean \pm SD shown, one-way ANOVA for significance[#]. 1 data point is the mean of one individual donor in a specific experiment.

E-G) Modified COMET assay with a representative plot of 1 experiment (E) and the combination of 3 different experiments (F), showing the relative tail moment in the COMET assay, illustrating the increased 8-oxoG in TH1579 treated cells. One-way ANOVA with Šídák's multiple comparisons test was performed significance[#].

#* = $p \leq 0.05$; ** = $p \leq 0.01$; *** = $p \leq 0.001$; **** = $p \leq 0.0001$.

Figure 5: MTH1 inhibition of activated T cells with TH1579 selectively kills MTH1^{high} T cells and increases the ratio of proliferating MTH1^{low} T cells.

A-B) Representative dot plots with adjunct histograms (A) and Quantifications (B) for the fraction of MTH1 positive T cells treated with TH1579 for 24h (CD3/CD28/IL-2 stimulated for 96h prior to treatment), illustrating the specific sensitivity of MTH1^{high} cells to MTH1 inhibition by TH1579, and the existence of proliferating MTH1^{low} cells in S and G2/M phase that are less sensitive. MTH1 FMO control (no primary MTH1 antibody added) to illustrate gating strategy and as a technical quality control. 2-way ANOVA with Dunnett's multiple comparisons test for significance[#] (B).

C) Histograms with PI of MTH1^{high} vs. MTH1^{low} cells to illustrate the cell cycle phases of both T cell types. The sizes of the histograms correlate to the number of cells per sample.

D-E) Quantifications of cells in G1 (D) and >G1 (S/G2/M) (E) for MTH1^{high} and MTH1^{low} cells, respectively and compared to DMSO. The G1 population is defined as the first peak in C and >G1 as the cells to the right of G1 in the histogram. 2-way ANOVA with Dunnett's multiple comparisons test for significance[#].

F-G) Comparison of the cell cycle in the vehicle control cells with resting cells (MTH1^{low}), activated MTH1^{high} and activated MTH1^{low} cells, to pinpoint the distinction between the MTH1^{low} cells and resting cells. One-way ANOVA with Šídák's and Tukey's multiple comparisons test for significance[#].

In B and D-G the combined mean \pm SD of different experiments is shown, where 1 data point is the mean of one individual donor in a specific experiment.

#* = $p \leq 0.05$; ** = $p \leq 0.01$; *** = $p \leq 0.001$; **** = $p \leq 0.0001$.

Figure 6: MTH1 inhibition with TH1579 drives the remaining surviving cells towards an MTH1^{low} phenotype with decreased ROS levels

A) Schematic overview of the handling of the cells in B-F, where the T cells were stimulated and treated with inhibitor simultaneously.

B-C) Dot plots (B) and quantifications (C) of the redox status and MTH1 levels in activated T cells after 96h of stimulation and simultaneous drug treatment, with DMSO as a control and the resting cells for reference. Mean \pm SD of material from different experiments and different individuals shown in bar charts, where 1 data point is the mean of 1 individual donor. Ordinary one-way ANOVA with Dunnett's multiple comparisons test performed for significance[#] as compared to DMSO for MTH1 and ROS levels, separately.

D) Quantification of the remaining living cells after treatment as presented in A, illustrating that the treated living cells investigated constituted a smaller number than the untreated cells. Mean \pm SD shown, combined from different experiments, where 1 data point is the mean of 1 individual donor. Ordinary one-way ANOVA with Dunnett's multiple comparisons test performed for significance[#] as compared to DMSO.

E) MTH1 expression per cell generation ("Gen") 0-4 in living cells after 96h of treatment, dot plots illustrating the number of cells in the different generations (density of dots) and difference in MTH1 intensity over the generations, as quantified in F. Only live single cells are gated for.

F) Quantification of E, as relative MFI values normalized to DMSO (1.0). Mean \pm SD shown, combined from different experiments, where 1 data point is the mean of 1 individual donor. Two-way ANOVA with Dunnett's multiple comparisons test performed for significance[#] as compared to the "Gen 0" control of each treatment group.

[#]* = $p \leq 0.05$; ** = $p \leq 0.01$; *** = $p \leq 0.001$; **** = $p \leq 0.0001$.

Figure 7: Non-toxicity in other immune cells

A-B) Quantification of phagocytosed cells (% of total) for Neutrophils (A) and Monocytes (B). Cells kept at 4°C as positive control. For significance[#], one-way ANOVA compared to the DMSO control was used.

C-D) Quantification of oxidative burst as MFI (absolute values) of dihydrorhodamin for Neutrophils (C) and Monocytes (D). Cells kept at 4°C as positive control, as well as Apocynin. For significance[#], one-way ANOVA compared to the DMSO control was used.

E-F) Cytotoxicity of NK cells with (E) and without (F) IL-2 stimulation, presented as % of lysed target cells. For significance, one-way ANOVA compared to the DMSO control was used.

G) Schematic overview of the KLH immunization study design, as described thoroughly in the materials and methods section.

H-I) Absolute values of the primary IgG response (H) and secondary IgG response (I) in the different groups presented in G. The non-parametric Mann-Whitney U-test test was used to compare all considered groups. For each pairwise group comparisons of interest, significance was reported at 95% significance level (corresponding to $p < 0.05$)

J-K) Absolute values of the primary IgM response (J) and secondary IgM response (K) in the different groups. The non-parametric Mann-Whitney U-test test was used to compare all considered groups. For each pairwise group comparisons of interest, significance was reported at 95% significance level (corresponding to $p < 0.05$)

Figure 8: Animal studies suggest a therapeutic role of TH1579 in the T cells driven disease model of multiple sclerosis, Experimental autoimmune encephalomyelitis (EAE)

A-B) Clinical and cumulative score in animals treated with TH1579 from either day 1 (n = 8) or the onset of symptoms day 12 (n = 7), as compared to the vehicle control (n = 8). Mean + SD shown. Two-way ANOVA with Dunnett's multiple comparisons test performed for significance[#] in A, where the TH1579 treated groups are compared to the control of the same time point. Ordinary one-way ANOVA performed in B for significance[#], as compared to the control.

C) EAE induction for 23 days and quantified limb paralysis. 2 separate experiments shown in the same graph, where n = 7 and 8 respectively in the two experiments for each group (control in grey and TH1579 in black). Mean + SD shown. Two-way ANOVA with Šídák's multiple comparisons test was performed for significance[#], comparing the test group to its own paired control for every day within the two separate experiments.

D) Splenocytes from D were cultured *in vitro* and stimulated with either MOG or ConA, quantification of proliferation shown. Mean ± SD shown, 1 data point is 1 spleen. Multiple t-tests performed for significance[#], as compared to the control samples.

[#]* = p ≤ 0.05 ; ** = p ≤ 0.01 ; *** = p ≤ 0.001 ; **** = p ≤ 0.0001.

Figure 1

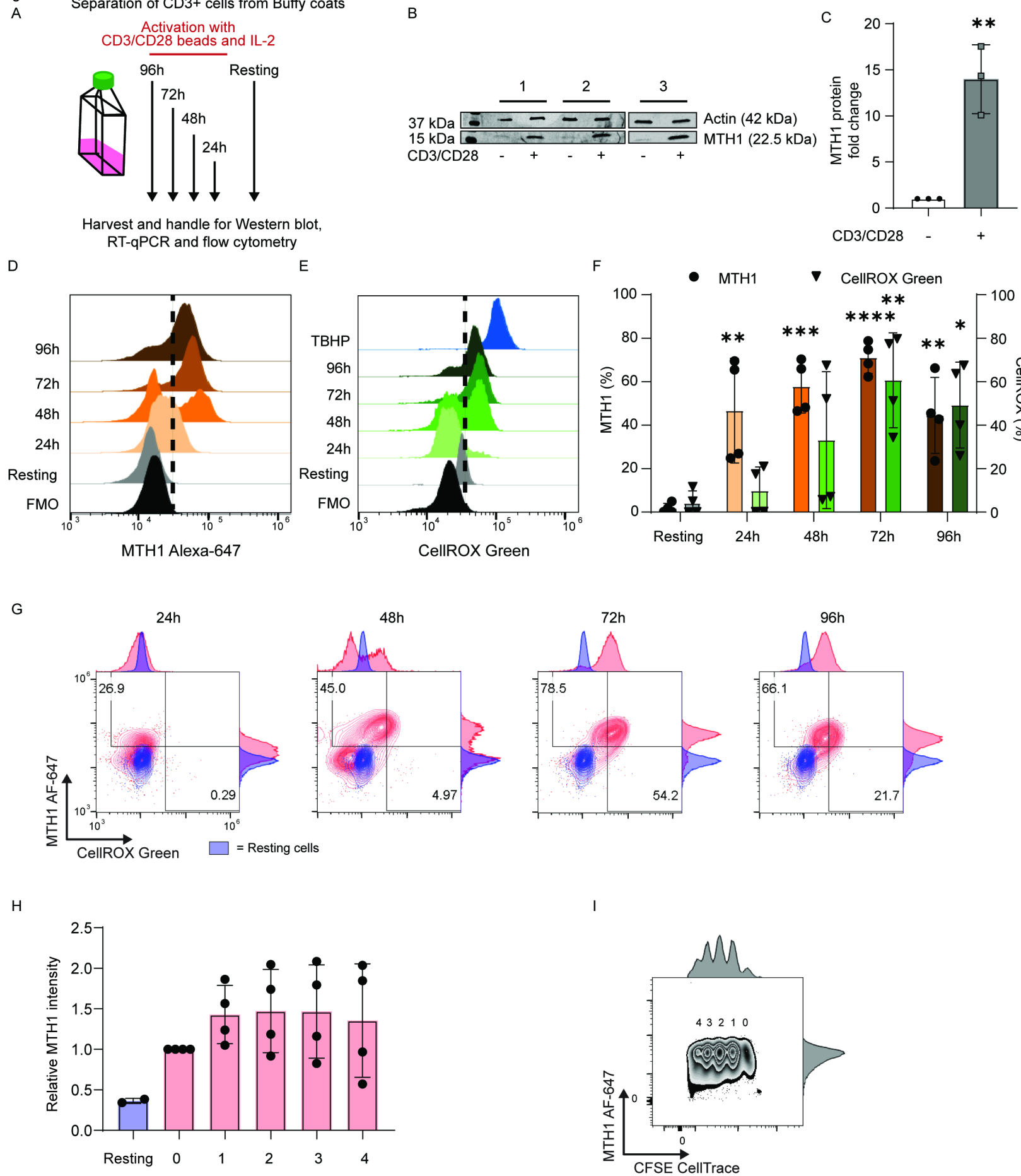


Figure 2

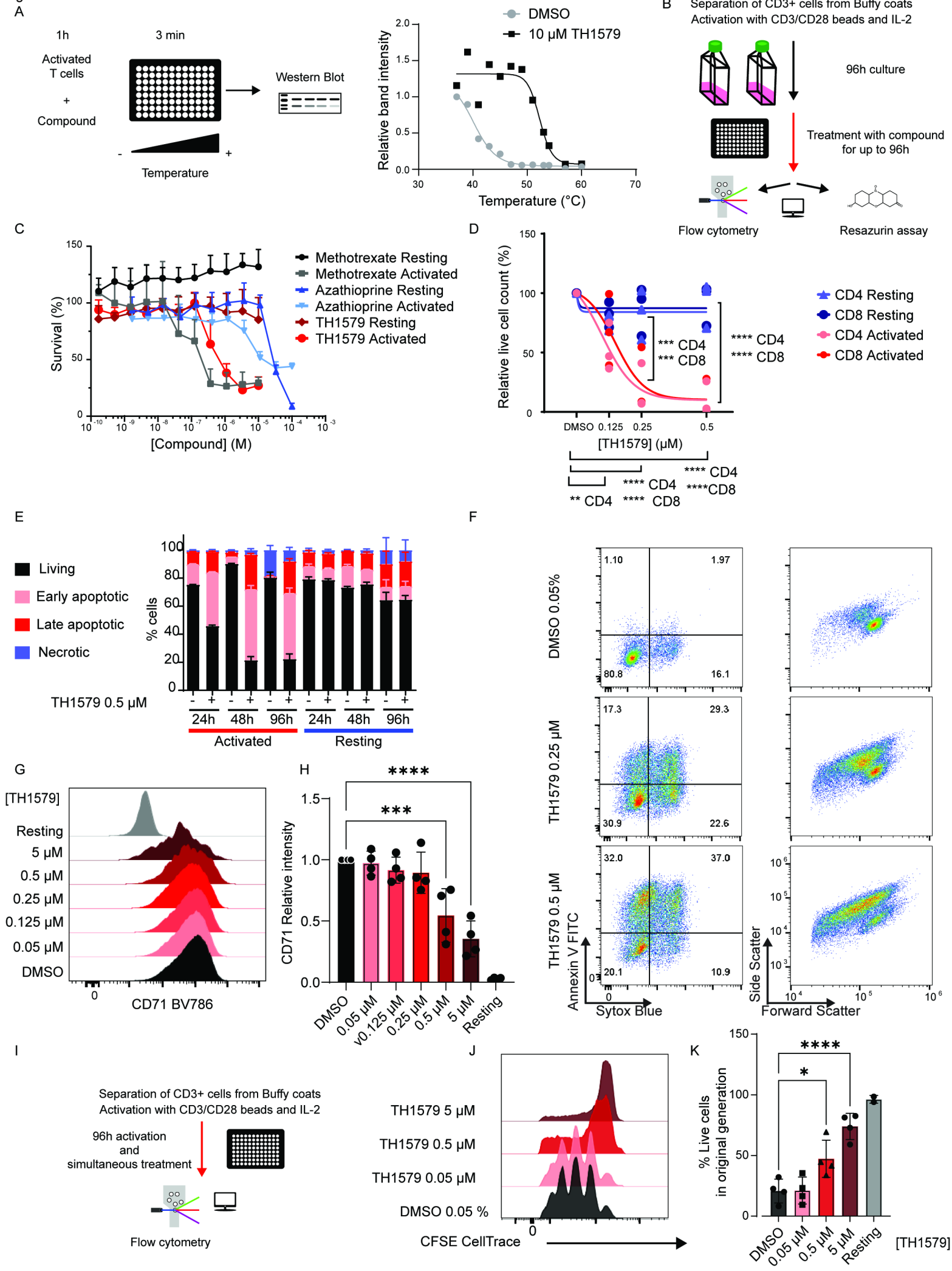


Figure 3

A Separation of CD3+ cells from Buffy coats
Activation with CD3/CD28 beads and IL-2

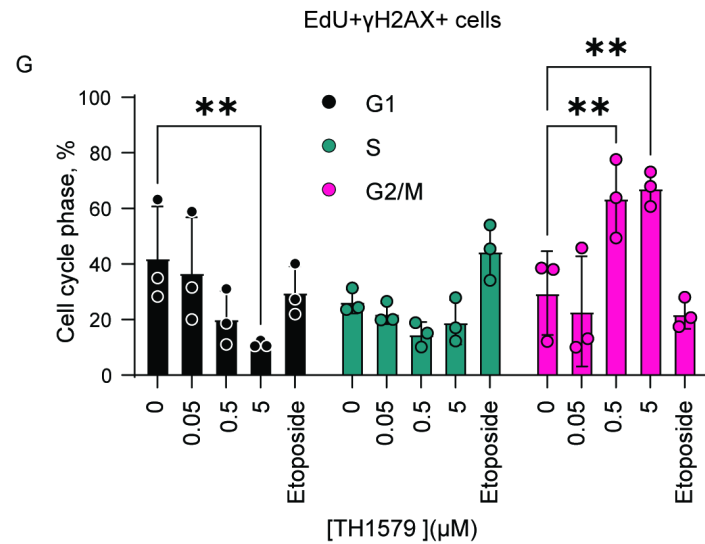
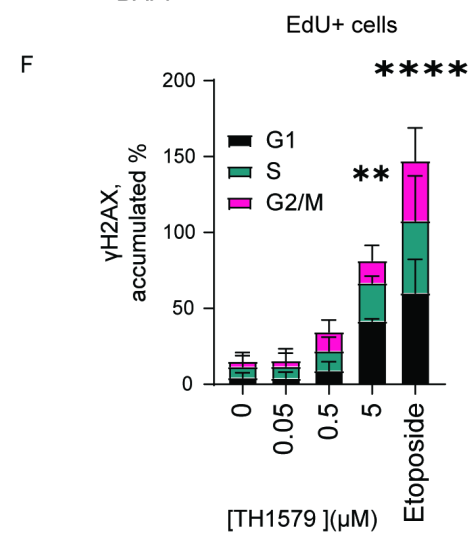
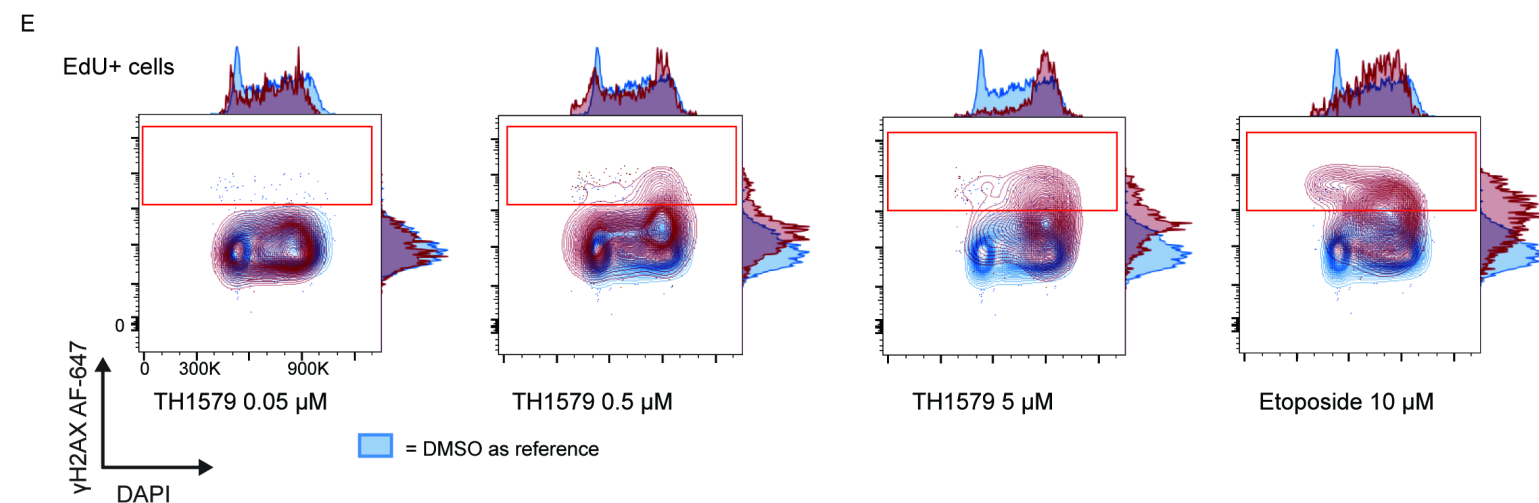
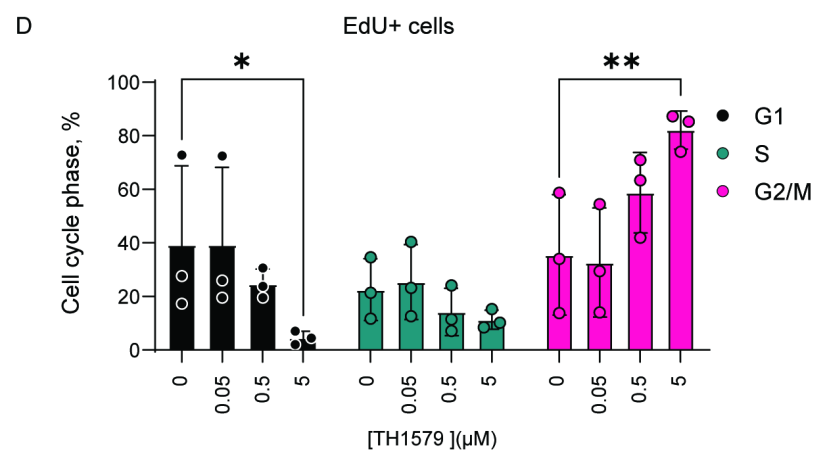
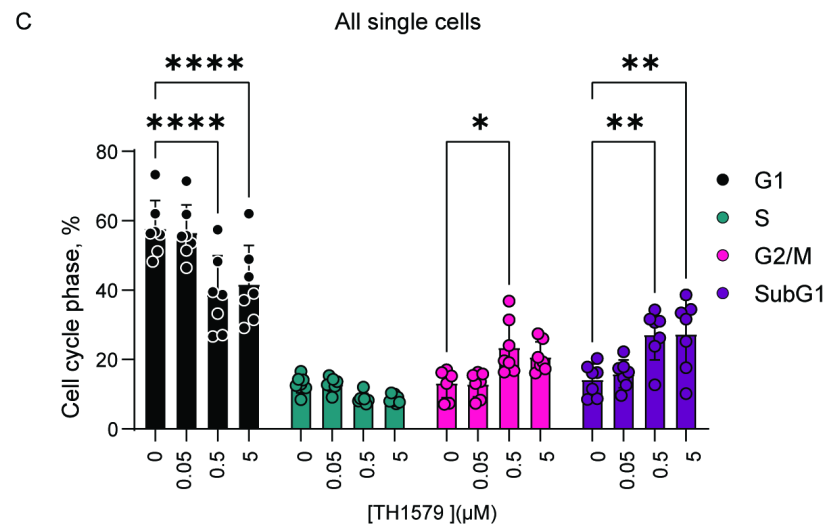
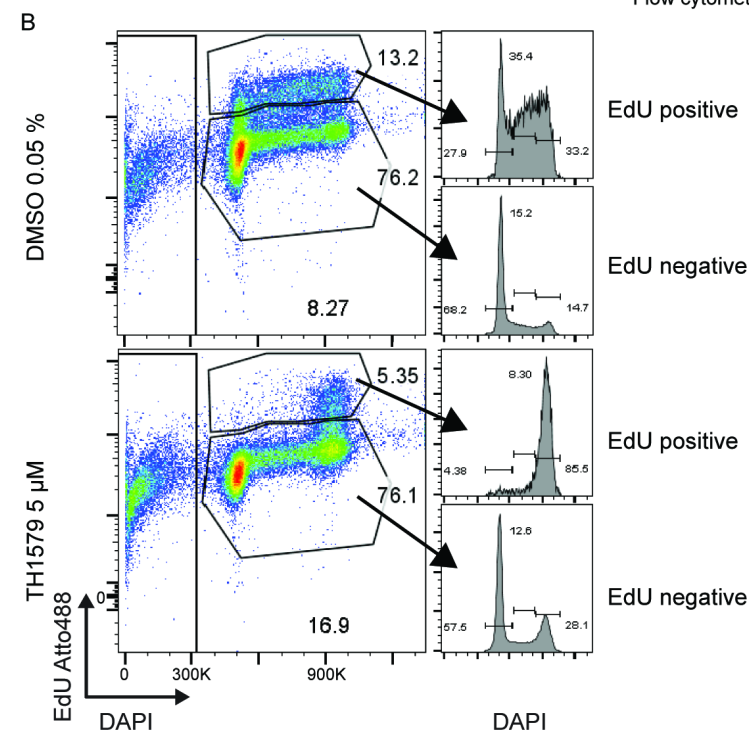
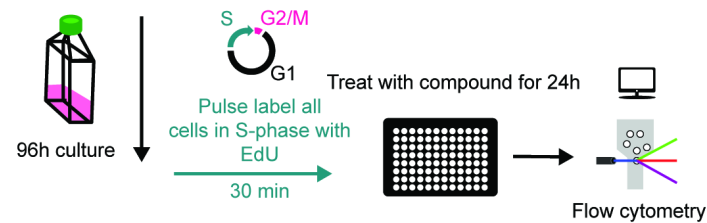


Figure 4

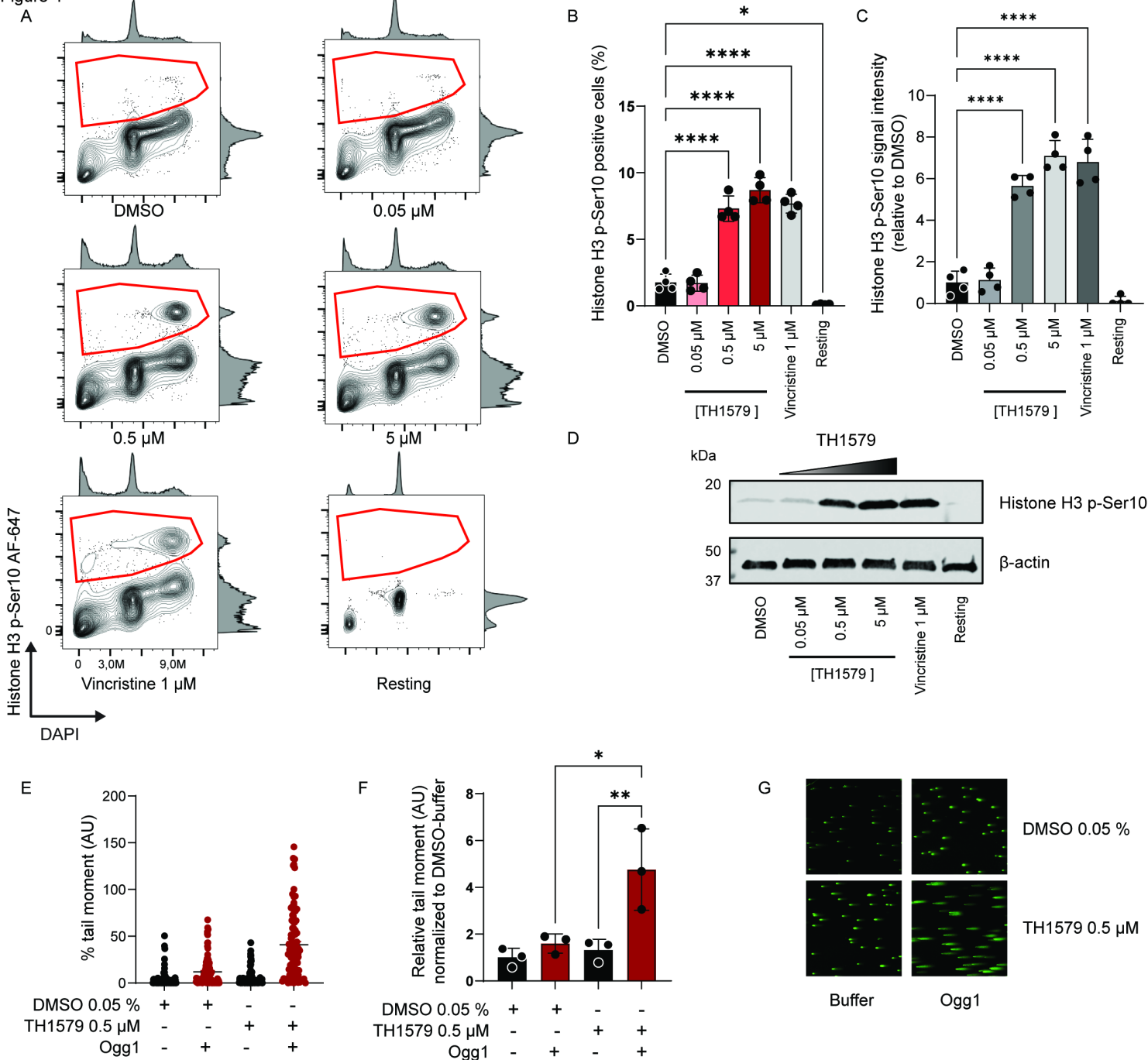
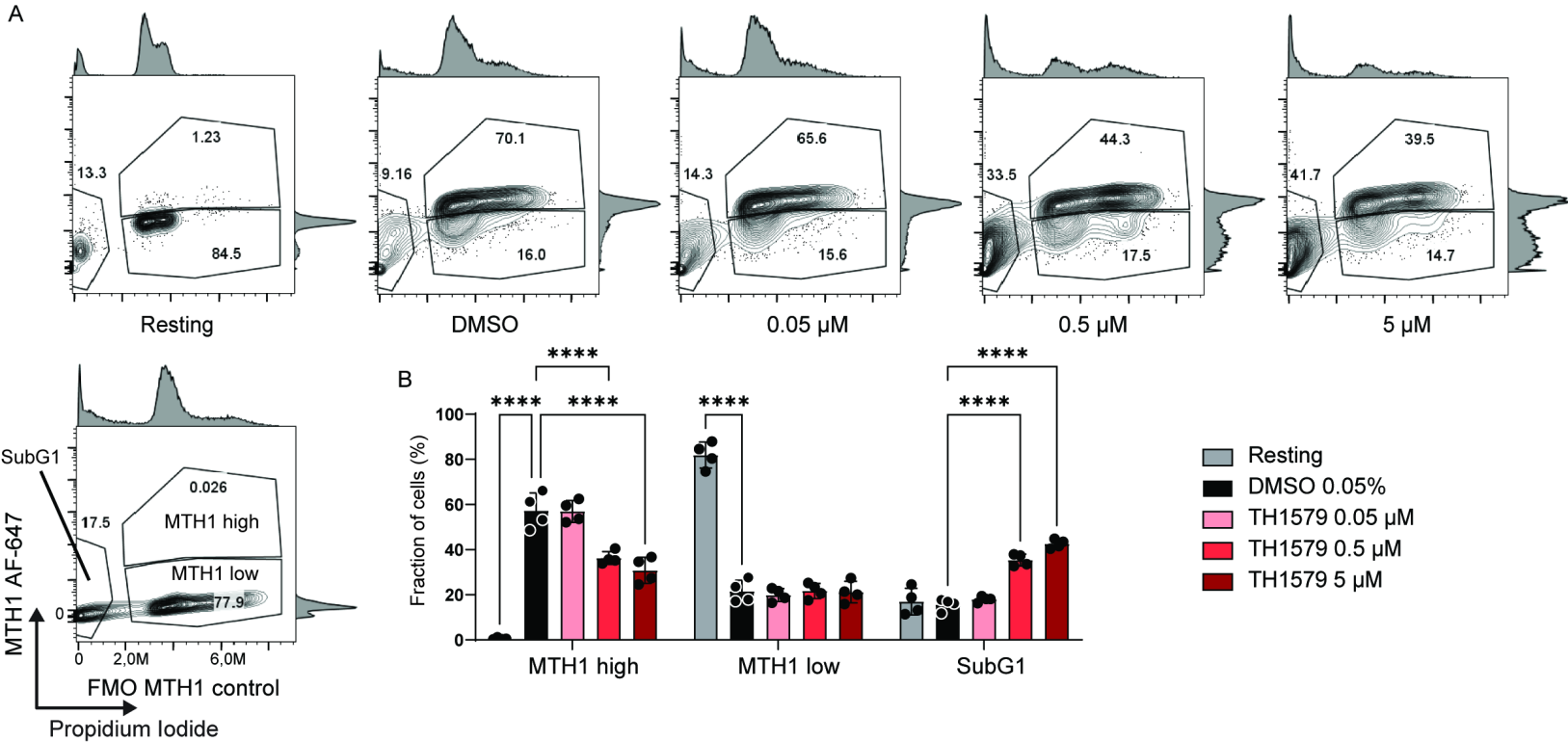
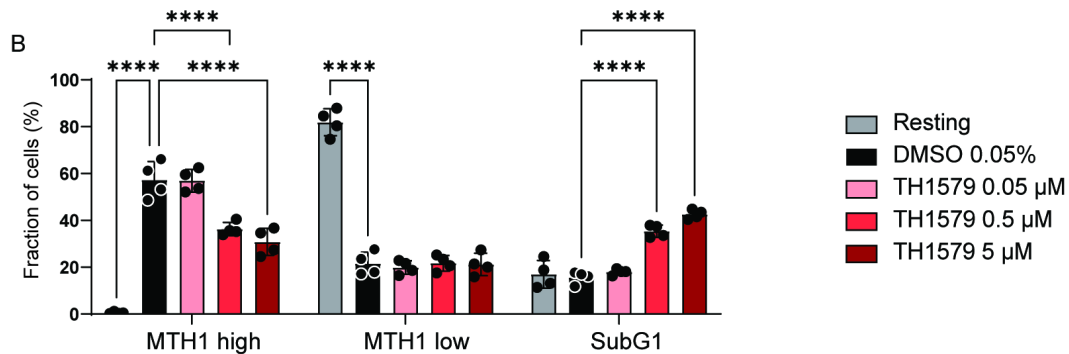


Figure 5

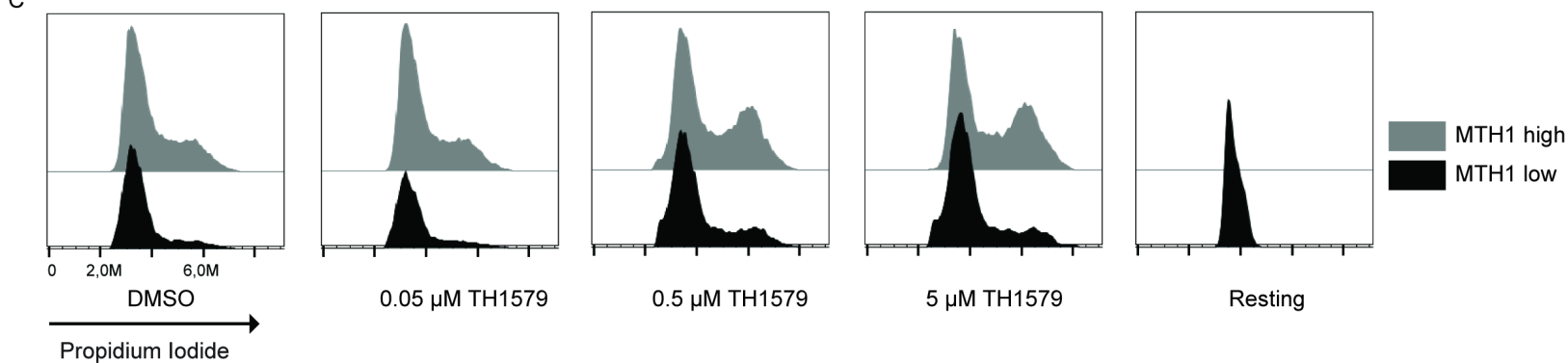
A



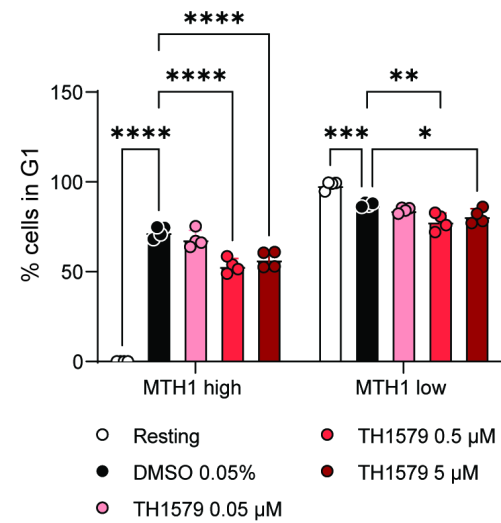
B



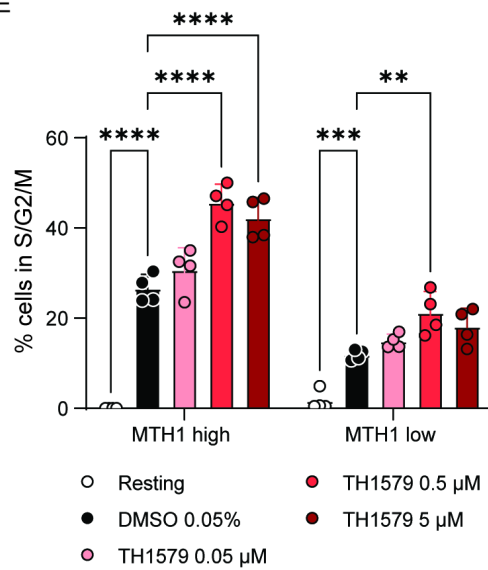
C



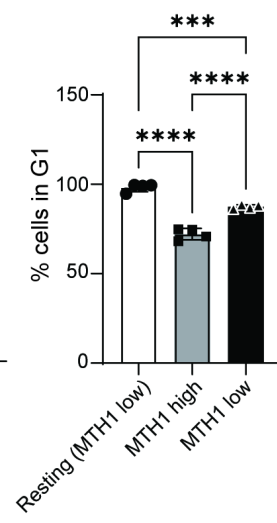
D



E



F



G

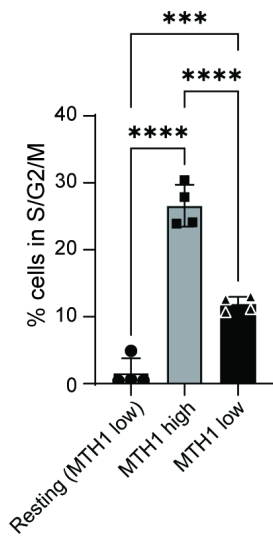
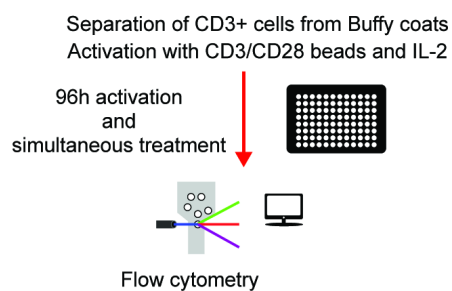
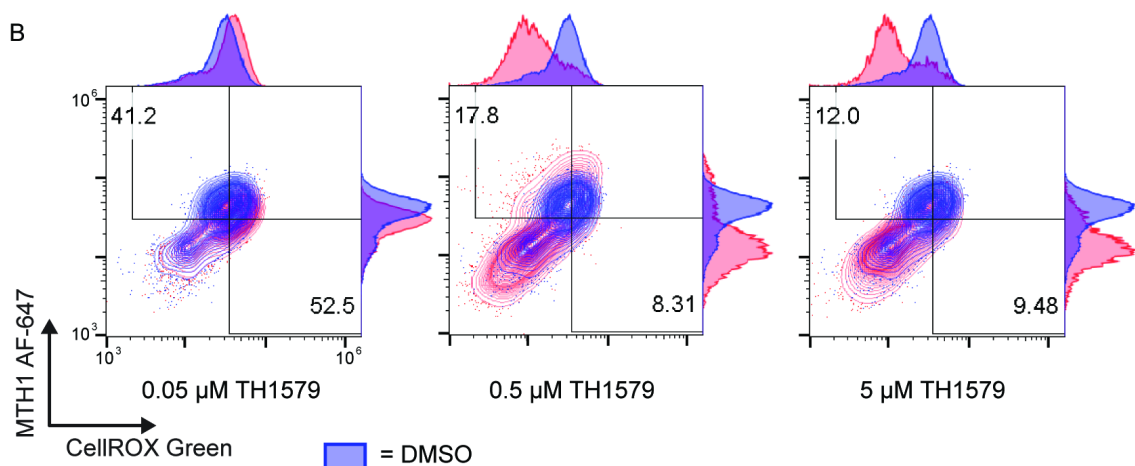


Figure 6

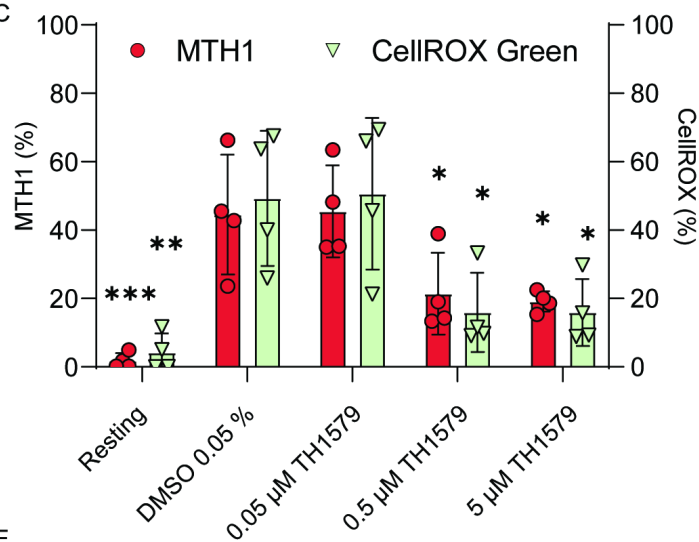
A



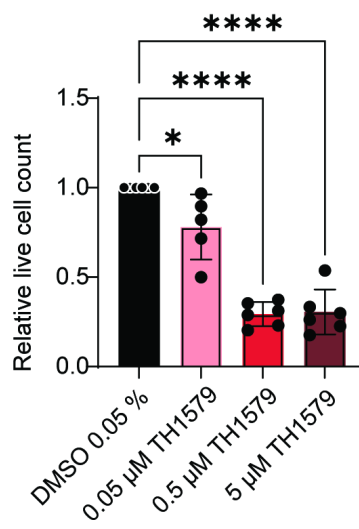
B



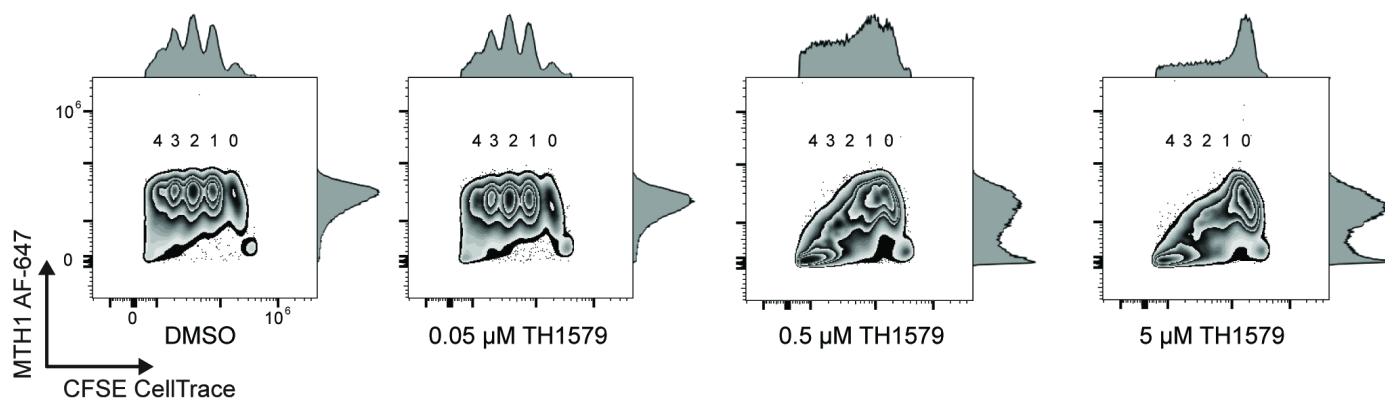
C



D



E



F

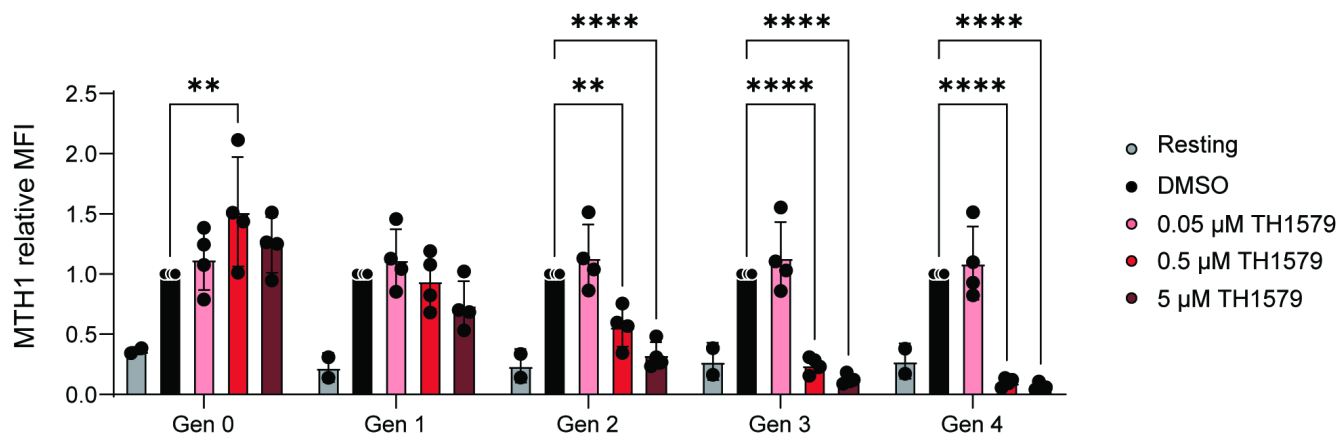


Figure 7

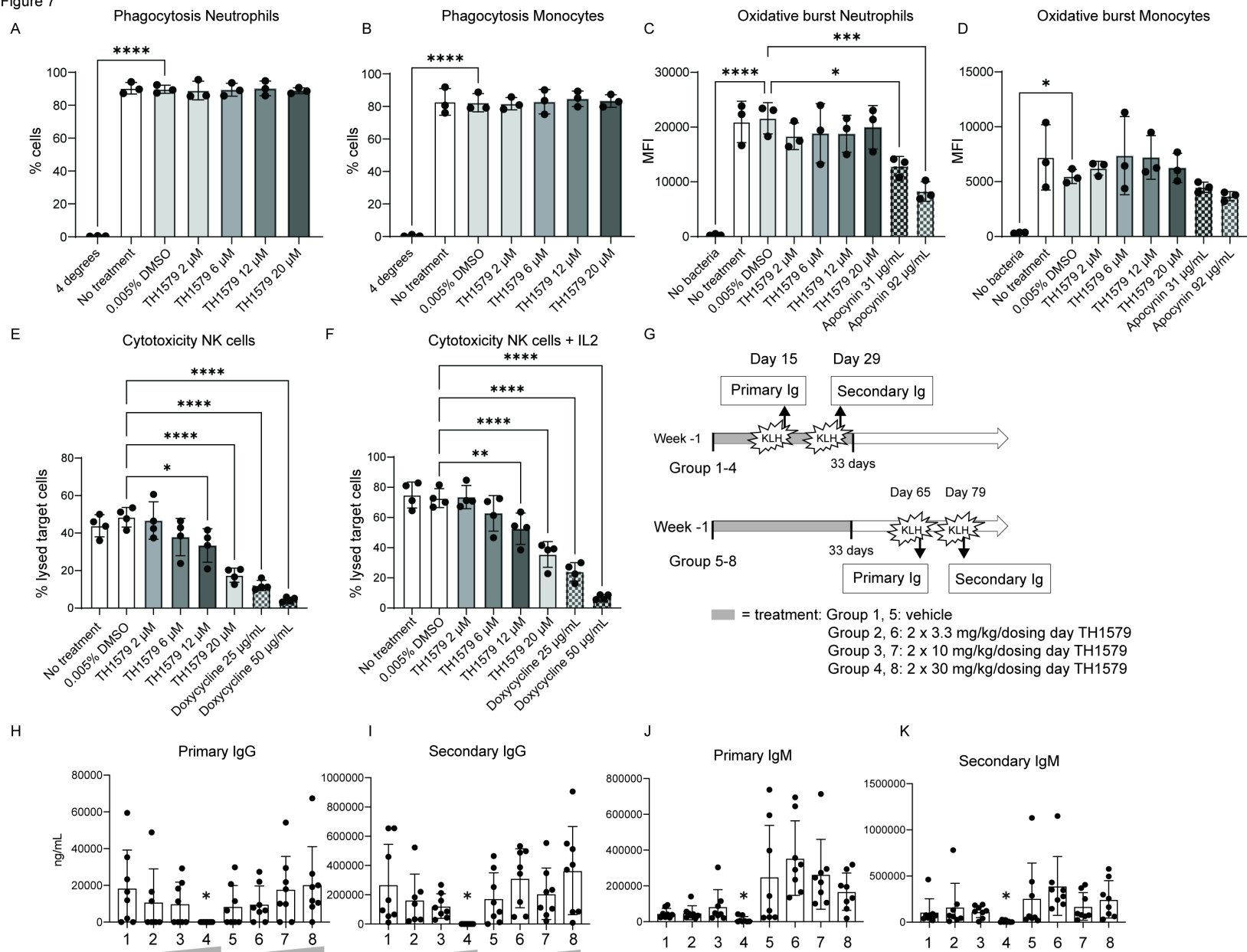
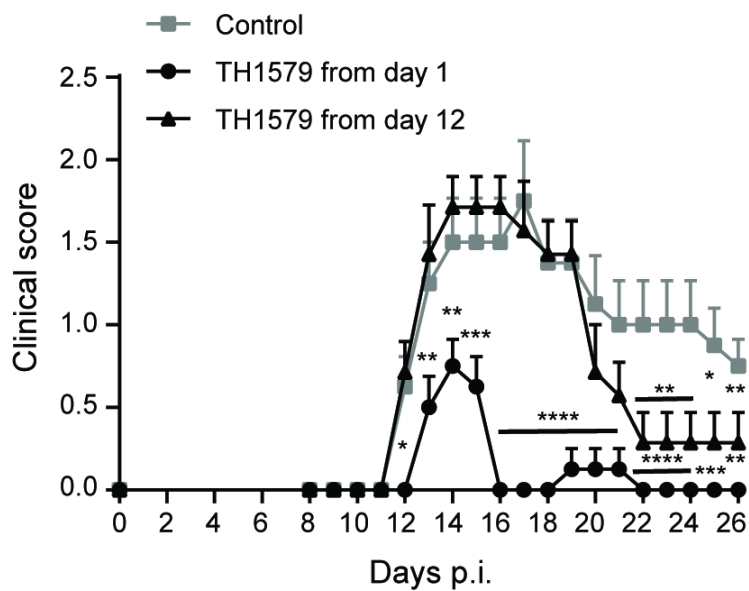
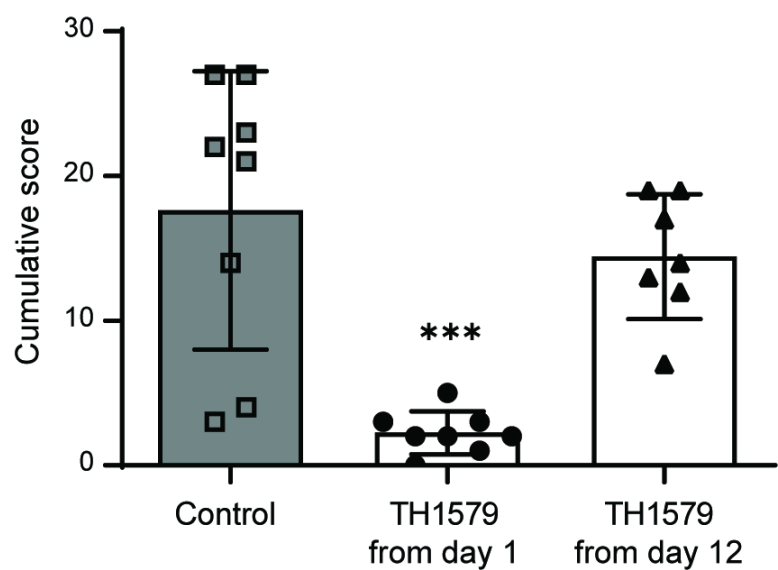


Figure 8

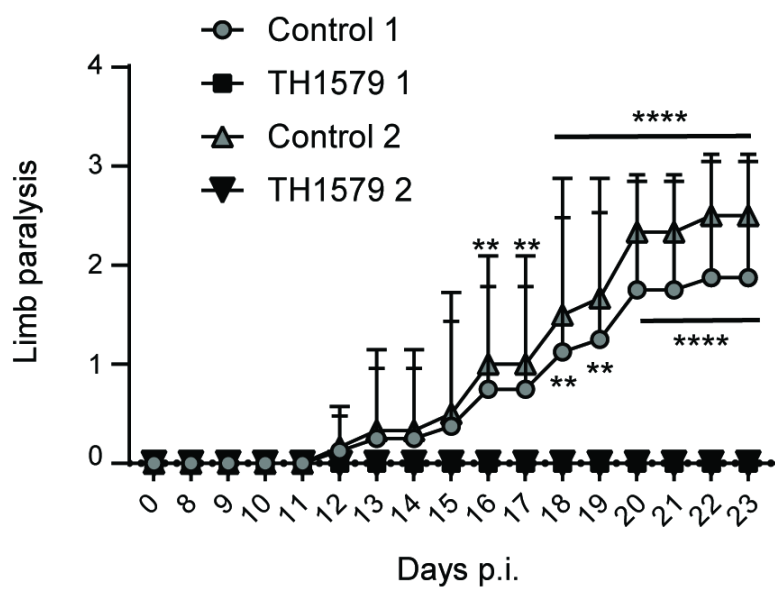
A



B



C



D

